Shipping Sunshine

A techno-economic analysis of a dedicated green hydrogen supply chain from the Port of Sohar to the Port of Rotterdam

Rogier Elmer Roobeek

Port of Rotterdam

TU Delft

Shipping Sunshine

A techno-economic analysis of a dedicated green hydrogen supply chain from the Port of Sohar (Oman) to the Port of Rotterdam (The Netherlands)

R.E. Roobeek (4614291)

In partial fulfillment of the requirements for the degree of:
Master of Science in Sustainable Energy Technologies

Course:
Graduation Project (SET3901)
First supervisor:
Prof. Dr. A.J.M. Wijk

Thesis committee:
Prof. Dr. A.J.M. van Wijk
Dr. E.G.M. Kleijn
Dr. ir. G. Korevaar

Delft University of Technology, The Netherlands

14th May 2020

Preface

Ever since I started my bachelors, I have felt the urgency of understanding and exploring different disciplines. It allowed me to attend courses ranging from international relations, to entrepreneurship and finance, to power and energy engineering. Seeking the complete horizon instead of just a picture of how to understand the world. Occasionally, this made people think it was due to a reality distortion field. In fact it might was.

During the lectures in the MSc Sustainable Energy Technologies and the MSc Industrial Ecology it became clear the world would only need a small area somewhere in the Sahara to harvest enough energy to power the world. To some it might be hard to believe, the real challenge is how to transport this tremendous renewable resource. Being confronted with the sheer size of the fossil fuel imports in Rotterdam and the resulting climate impact, the link was made: shipping sunshine.

It would not have been possible without the support from both the Port of Rotterdam as well as my supervisors at the TU Delft. I am grateful they embarked with me on this journey of exploring a part of the horizon that has not been explored yet. A special thank you to Ankie Janssen, Randolf Weterings, Dr. E.G.M. Kleijn and Prof. Dr. A.J.M van Wijk, who had confidence in setting up this research. Besides, I would like thank my family and friends who sparked my motivation even further.

Abstract

The Port of Rotterdam has the vision to become a zero-emission port in 2050. At the moment, the port area emits about 18% of Dutch CO_2 emissions. Various studies have been conducted on how to reach this vision. Among others, the Wuppertal Institute has investigated what set of technologies in each scenario would be desirable to employ. However, these studies were bound to the geographical context of the emissions. The tremendous impact of the up- and downstream flows was not included and is not included in the Dutch emission statistics. This thesis is the first element of a two-part analysis. In this part, a green hydrogen supply chain from the Port of Sohar towards the Port of Rotterdam will be taken as a case study in order to evaluate the current techno-economic potential of such a supply chain. The second part will evaluate which hydrogen markets in the hinterland of the Port of Rotterdam are feasible for the introduction of green hydrogen sourced from the Port of Sohar.

This green hydrogen supply chain is based on solar pv solely, in combination with electrolyzers, hydrogen storage, liquefaction and liquid hydrogen shipping. A cost model is proposed, that includes each stage of this supply chain. Finally, a price per kilogram of hydrogen is calculated. The price of hydrogen arriving in Rotterdam is found to be 2.17 [$\$ \cdot kg^{-1}$], including shipping.

Even though the price of green hydrogen arriving in Rotterdam is lower than the price of green hydrogen based on electrolysis produced locally, it is yet more expensive in comparison to grey or blue hydrogen produced in the Netherlands. However, economies of scale have not been included in this analysis, neither the potential of cost optimization throughout this supply chain. Therefore, future research is required to evaluate further cost reduction potential in this supply chain.

Keywords Green hydrogen, Techno-economic analysis, Renewable energies, Water electrolysis, Green hydrogen economy

Contents

List of Figures

List of Tables

Nomenclature

List of abbreviations

Symbol	Description
AEC	Alkaline electrolyzer
CCS	Carbon capture and storage
CCUS	Carbon capture, utilisation and storage
CSP	Concentrated solar power
DC	Direct current
GHG	Greenhouse gas
ICV	In country value
IEA	International Energy Agency
LNG	Liquefied natural gas
LOHC	Liquid organic hydrogen carriers
PEMEC	Proton exchange membrane electrolyzer
PEMFC	Proton exchange membrane fuel cell
PEX	Pressure exchanger
PoR	Port of Rotterdam
PoS	Port of Sohar
SMR	Steam methane reforming
TEA	Techno-economic analysis

List of greek symbols

Symbol	Description	Units
β	Tilt angle	[°]
γ	Shadow angle	[°]
ρ	Density	$[\mathrm{kg} \cdot \mathrm{m}^{-3}]$

List of roman symbols

Symbol	Description	Units
$Annuity$	Annuity	[-]
$Capacity$	Capacity to be realized	[-]
$CAPEX$	Capital expeniture	[$]
$Capacity_{\mathrm{nominal}}$	Capacity nominal	[-]
Cp	Capacity factor	[-]
D	Diameter of the pipeline	[m]
d	Spacing modules	[m]
E_{HHV}	Higher heating value hydrogen	$[\mathrm{kWh} \cdot \mathrm{kg}^{-1}]$
f_{cap}	Overcapacity factor	[-]
$fixOPEX$	Fixed operational expenditure	[$]
FLH	Full load hours	[-]
f_{prod}	Overproduction factor	[-]
h	Height modules	[m]

$Invest_{\text{base}}$	Base investment	[$]
$Invest_{\text{compare}}$	Comparison investment	[$]
$Invest_{\text{scale}}$	Scaling parameter	[-]
$Invest_{\text{total}}$	Total investment	[$]
$LCOE$	Levelized cost of electricity	$[\$ \cdot \text{kWh}^{-1}]$
$LCOH$	Levelized cost of hydrogen	$[\$ \cdot \text{kg}^{-1}]$
M_{b}	Brine flow	$[\text{m}^3 \cdot \text{day}^{-1}]$
M_{d}	Permeate flow	$[\text{m}^3 \cdot \text{day}^{-1}]$
M_{f}	Feed flow	$[\text{m}^3 \cdot \text{day}^{-1}]$
N_{ship}	Number of ships	[-]
OM	Operation and maintenance	[%]
$OPEX$	Operational expeniture	[$]
P	Power hydrogen pipeline	[MW]
RR	Recovery rate	[-]
$TOTEX$	Total expenditure	[$]
$varOPEX$	Variable operational expenditure	[$]
v_{H2}	Velocity hydrogen	$[\text{m} \cdot \text{s}^{-1}]$
$WACC$	Weighted average cost of capital	[%]
w	Width modules	[m]

1 Introduction

Recently, the Port of Rotterdam (henceforth PoR) committed itself to a substantial emission reduction pathway following the Paris agreement outcome. By 2025, the PoR wants to reduce its CO_2 emissions by as much as 50% (Samadi et al., 2017a). Moreover, the PoR has the ambition to become a zero emission port in 2050 (Port of Rotterdam, 2017). This has tremendous consequences for the activities that are performed within the port area. However, these ambitions do not cover the associated emissions of the energy throughput of the PoR (Samadi et al., 2017a).

The PoR plays a very important role as an energy port, not only for the Netherlands, but also for Europe. Besides the consumption of energy in the port area for industrial usage, the port area has the function of an energy hub, importing and exporting vast quantities of energy. In 2018, about 8,802 [PJ] of energy (primarily fossil) was imported and exported overseas in the port area, while 5,146 [PJ] was imported and exported to and from the hinterland of the port (Melieste, 2019). Since the primary energy consumption (including losses in industry) in the Netherlands is 3,100 [PJ], the import plus export overseas is about 3 times the primary Dutch energy consumption (CBS, 2019).

These up- and downstream energy flows are transformed in some cases into different energy carriers, in other cases they are simply transshipped unaltered. However, they all have their own use in the hinterland of the port. Some of the energy flows are used as kerosene at airports, other flows consist of coal and are used as a feedstock for the steel industry (Melieste, 2017). Hence, it becomes clear that each of the energy flows has a different CO_2 intensity, as the emission factors of energy carriers varies substantially (Vreuls, 2004). Moreover, each energy demand has its own characteristics.

Aim and research questions This research consists of two parts. The aim of this first part is to evaluate whether the energy demands in the hinterland of the PoR could become less CO_2 intensive, by analysing the current techno-economic feasibility of setting up a green hydrogen supply chain. The PoR will be taken as a case study in order to evaluate the potential of green hydrogen transshipment activities within the port area sourced from the Port of Sohar (henceforth: PoS). The PoS is chosen as a focal point for two main reasons: Oman has plentiful renewable resources from which green hydrogen could be produced, the PoR has a 50% stake in the the PoS (Kazem et al., 2015; Van Den Bosch et al., 2011). Hence, the main research question is: *what is the current techno-economic feasibility of setting up a green hydrogen supply chain between the Port of Sohar and the Port of Rotterdam?*

The following sub-questions will be addressed consecutively, where supply chain stages are understood as echelons in the supply chain that contribute to the levelized cost of hydrogen:

- What could be learnt from literature regarding renewable energy technologies in the context of green hydrogen supply chains?
- What would be a techno-economic feasible configuration for setting up a green hydrogen supply chain, given the conditions in Oman?
- What parameters are representative for each supply chain stage?

- What would be the levelized cost of hydrogen arriving in Rotterdam?
- How do the most cost contributing stages influence the levelized cost of hydrogen?

The second part of the research focuses on identifying and evaluating which energy throughputs through the port area are feasible to be substituted by green hydrogen, or alternatively which energy throughputs could develop in the future that could create new demand for imported green hydrogen in the PoR. It will instead be in partial fulfillment of the MSc Industrial Ecology. Nevertheless, this master thesis will be in partial fulfilment of the MSc Sustainable Energy Technologies and it will focus on the Sohar side of this conceptual supply chain.

The study has the following structure. In Chapter 2, both the social and the scientific knowledge gap will be addressed. Afterwards, in Chapter 3 the research approach and methodology will be covered and elaborated upon. Thereafter, Chapter 4 will provide for the results. Finally, Chapter 5 and Chapter 6 will address both the discussion and the conclusion. Ultimately a recommendation will be given. Lastly, the assumed data (e.g. assumptions for the cost model) is put in Appendix A and an overview of the cost factors is provided in Appendix B.

2 Literature review

As mentioned in Chapter 1, a port authority could have substantial influence on the sustainability of the up- and downstream flows that flow through the port area towards the hinterland of the port. Besides, Rotterdam fulfills an important function in transshipping large amounts of energy carriers (Melieste, 2017).

A German research institute, the Wuppertal Institute, developed four scenarios for the PoR on how the port could realize its vision to decarbonize the industrial activities in the port area. Furthermore, the institute made the following recommendation in the report:

It needs to be mentioned that – although this study is limited in scope to the industrial activities and to the related territorial emissions in the port area – it is obvious that the huge up- and downstream flows and transports of resources, energy and products that are linked to the industrial as well as logistics activities also have significant impacts on global GHG emissions and resource depletion. Via their influence on these flows and the linked value chains, the port and its industries hold an important lever for climate mitigation outside of their territorial boundaries. These options should also be systematically explored in the future and should be included in an overall decarbonization strategy for the port (Samadi et al., 2017b).

Hydrogen could play a key role in making the energy throughput in the PoR more sustainable, especially when different energy markets are able to switch from fossil energy carriers to green hydrogen (e.g. steel industry, chemical industry, mobility). There are three different kinds of hydrogen: grey hydrogen, blue hydrogen as well as green hydrogen. Although these three alternatives are respectively declining in their greenhouse gas (GHG) impact, each could help in the transition towards a low carbon energy throughput in the PoR.

In Section 2.1, hydrogen will be evaluated from a market perspective. Subsequently, Section 2.2 will evaluate research on green hydrogen supply chains. Afterwards, the local characteristics of Oman will be explored in Section 2.3. Finally, the technologies that could be harnessed will be assessed in Section 2.4.

2.1 Hydrogen production

Grey hydrogen, which is fossil based and does not have the carbon capture and storage included, is little different from the fossil-based feedstocks that are currently used. Blue hydrogen is produced from fossil-based feedstocks, but the CO_2 emissions are reduced by a CCUS (carbon capture, utilisation and storage) facility. Green hydrogen on the other hand, is produced with renewable resources (e.g. biogas/biomass or green electricity) (IEA, 2015). As green hydrogen has the lowest emission factor, it will be this green feedstock that this research will focus on to lower the GHG impact of the downstream energy markets in the hinterland of the PoR.

While the ammonia market is globally well developed, there is no such thing as a global trade in hydrogen, primarily because of its transport being perceived costly. However, hydrogen itself is produced already for decades. It is produced both dedicated near the demand as well as created as a by-product (IEA, 2019). Dedicated production occurs mostly from (in descending order): natural gas, coal, oil and electricity. Besides there is by-product production

from for instance the chlor-alkali industry (see Figure 1). Hydrogen is used in (in descending order): refining, ammmonia, heat, methanol, DRI (direct reduction of iron), other and finally transport (IEA, 2019).

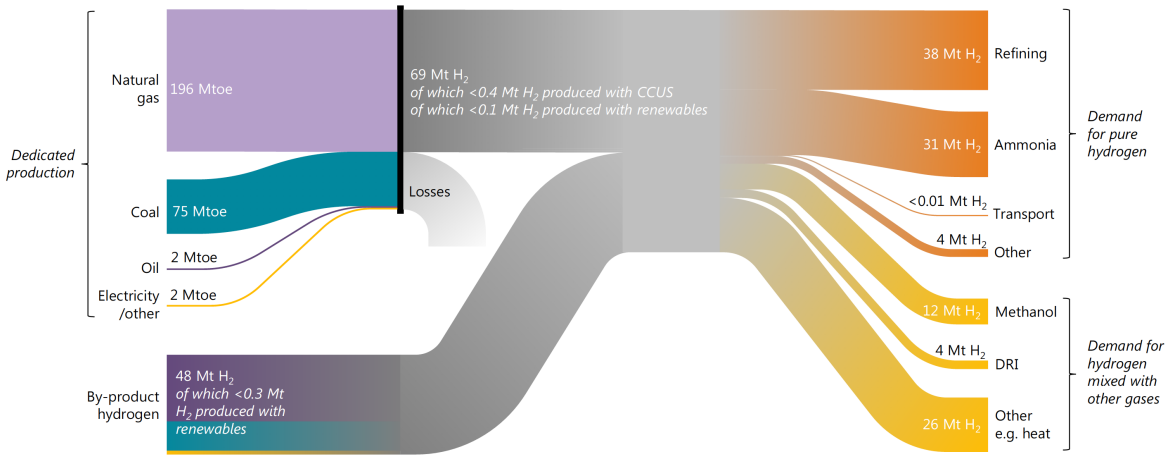

Figure 1: Overview of the production and consumption of hydrogen on a global scale in 2019(IEA, 2019).

It becomes clear that in today's market, natural gas is the main resource used as a feedstock for hydrogen production. Therefore, the hydrogen production cost based on natural gas will be substantiated for different regions by means of a graph. In Figure 2, a comparison is made between the price per kilogram of hydrogen for production from natural gas in different regions throughout the world. In the Middle East, the price of hydrogen is about 1.5 $[\$ \cdot \mathrm{kg}^{-1}]$ including CCUS, which does not include shipping or storage and is based on the current state of technology.

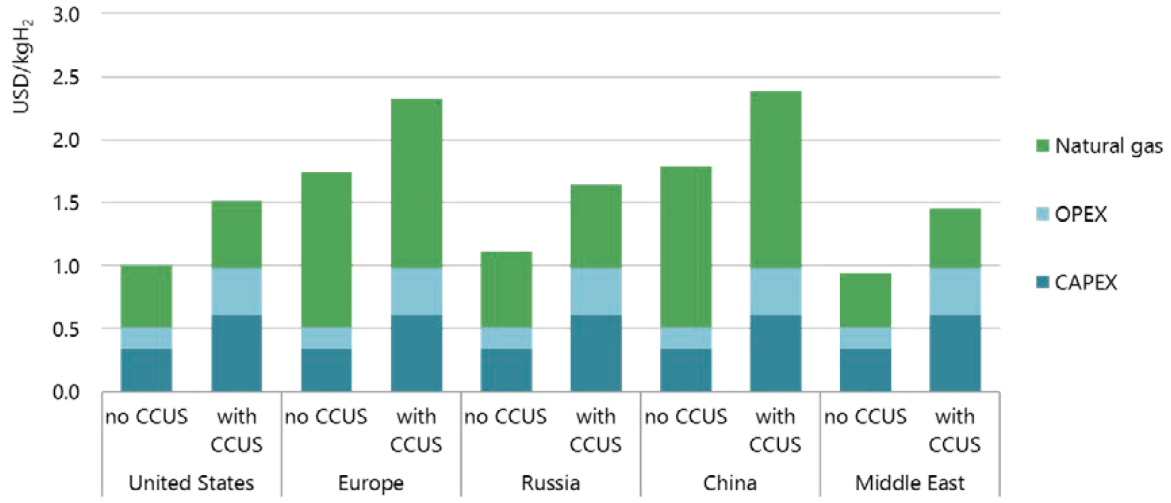

Figure 2: Comparison of hydrogen (blue and grey) from natural gas in different regions throughout the world (IEA, 2019).

It is important to note that the prices in Figure 2 are based on the following assumptions that vary regionally. The $CAPEX$ for the steam methane reforming (SMR) plant without carbon capture, utilisation and storage (CCUS) varies between 500 and 900 [$\$\cdot kW^{-1}_{H2produced}$]. On the other hand, the $CAPEX$ for the steam methane reform (SMR) plant with CCUS varies between 900 and 1600 [$\$ \cdot kW^{-1}_{H2produced}$]. In addition, the price of natural gas varies in Figure 2 between 3 and 11 [$\$ \cdot MBtu^{-1}$] (henceforth MBtu is million Btu) .

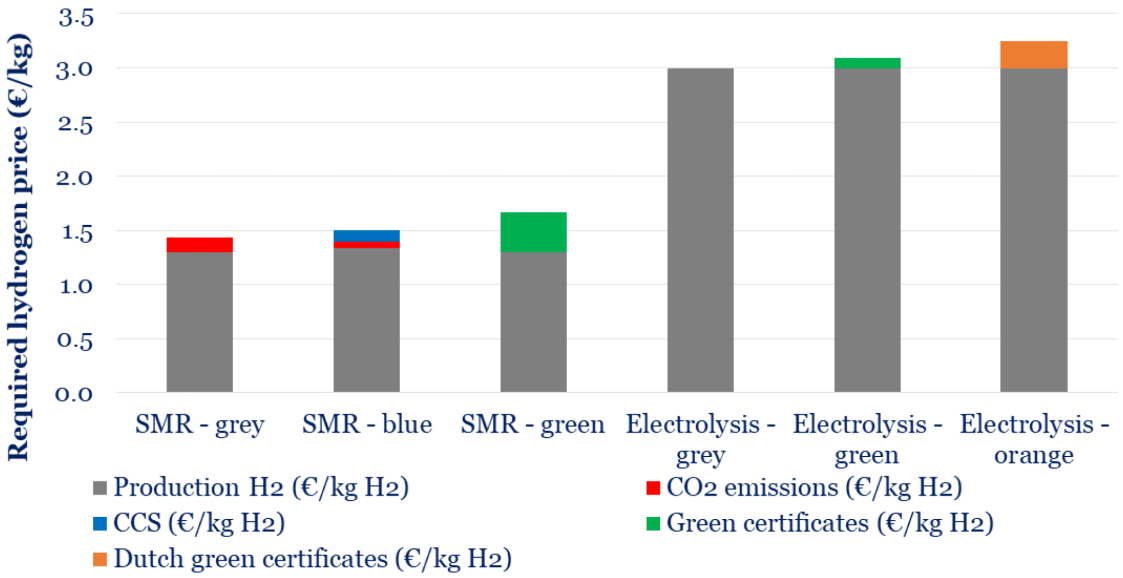

Figure 3: Hydrogen production cost in the Netherlands (Mulder et al., 2019).

Cost estimates have been made for the Netherlands as well. Mulder et al. evaluated the costs of different types of hydrogen. The results are depicted in Figure 3. The main underlying assumptions are the following. The price of natural is set at 20 [€·MWh^{-1}], which is converted about 6.45 [$\$\cdot MBtu^{-1}$]. Furthermore, the CO_2 price is set at 15 [€·t^{-1}] and the capture rate of 55% (Mulder et al., 2019). Further SMR plant assumptions are based on Collodi et al. (Collodi et al., 2017).

In addition, SMR-green is based on biogas, electrolysis grey uses grid electricity, electrolysis green uses green grid electricity and electrolysis orange uses Dutch green electricity (Mulder et al., 2019). Lastly, the main assumptions for the electrolysis based hydrogen is an electricity price of 47 [€·MWh^{-1}], a $CAPEX$ of 750 [€·kW^{-1}] for the electrolyzer and a premium for generic and Dutch renewable electricity of 2 and 5 [€·MWh^{-1}] respectively (Mulder et al., 2019).

To put this into perspective, the price of natural gas in Sohar ranges between 3.5 and 4 [$\$ \cdot MBtu^{-1}$] (Costa, 2019). Converted into Euro and [MWh], a price range of 11 and 12 [€·MWh^{-1}] is representative in Oman currently. When using the sensitivity analysis by Mulder et al, the price of grey hydrogen would be very close to 1.1 [$\$\cdot kg^{-1}$], and zero emission allowance costs (1.1 [€·kg^{-1}] with allowance costs, subtracting CO_2 allowance costs of 0.14 [€·kg^{-1}_{H2}] due to SMR emissions of 9.01 [$kg_{CO2} \cdot kg^{-1}_{H2}$] and multiplying with 1.1 [USD/EUR]) (Mulder et al., 2019). In that case shipping costs are not included, nor CO_2 emission costs.

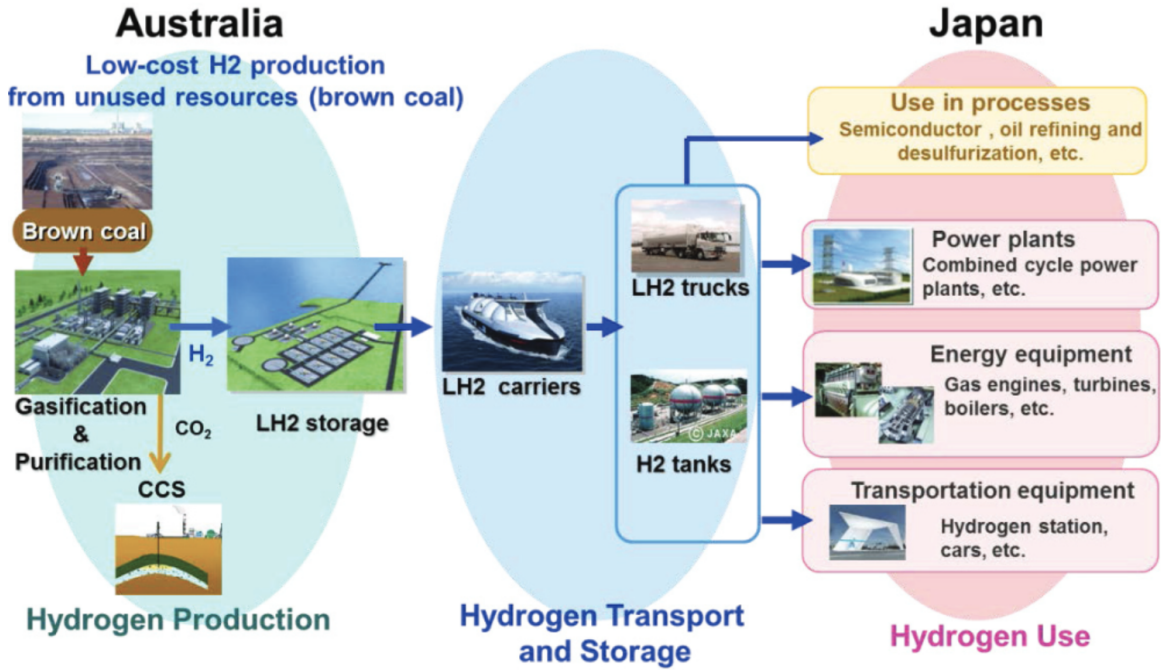

Figure 4: A hydrogen supply chain between Australia and Japan with its constituents (Kamiya et al., 2015).

Local hydrogen supply chains exist already for some time (Wijk, 2019b). However, globally there exist two key examples of overseas hydrogen supply chains that are currently in development: a hydrogen trade link between Australia and Japan and between Brunei and Japan.

In the former case hydrogen is produced from brown coal in Australia, CO_2 is stored making use of CCS (carbon capture and storage), hydrogen is liquefied, stored, shipped and subsequently used for various purposes. The conceptual supply chain is depicted in Figure 4. At the moment, a pilot of the supply chain between Australia and Japan is commenced. At a future commercial scale, a total annual supply of 0.225 [Mt] would be shipped to Kobe, Japan. At this commercial scale, using a conversion of 0.0092 [¥/$] and 11.1 [$\mathrm{Nm}^3 \cdot \mathrm{kg}^{-1}$], the total costs for hydrogen were derived in [$\$ \cdot \mathrm{kg}^{-1}$] (Kawasaki, 2019). The price built-up is depicted in Figure 5 by means of a waterfall chart. The total cost of one [kg] of hydrogen is found to be 3.05 [$\$ \cdot \mathrm{kg}^{-1}$], where the two most contributing cost factors are hydrogen production and hydrogen liquefaction.

In the latter case, hydrogen is bound to toluene in Brunei and dehydrogenated at the destination in Japan. The hydrogen would be produced by SMR. A total of 210 [t] of hydrogen is expected to be shipped in order to supply the Keihin refinery in 2020 (Yasui, 2018).

When considering green hydrogen, produced with renewable resources, it plays a minor role in the current hydrogen production. It is however not bound to fossil fuels, which raised the interest for domestic production, also in the Netherlands. As suggested in previous studies, this would require vast amounts of renewable electricity that would preferably first finds its way into the national electricity market (H-Vision, 2019).

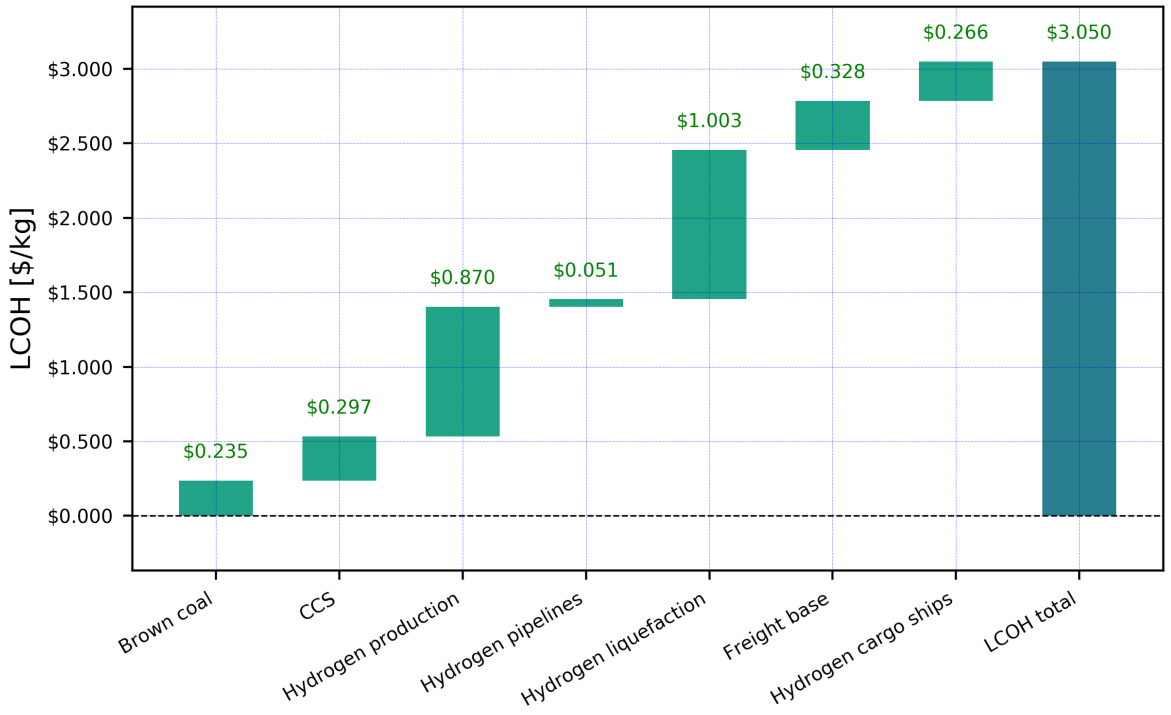

Figure 5: Decomposition of the levelized cost of hydrogen ($LCOH$) into its constituents in Japan [$\$ \cdot \mathrm{kg}^{-1}$].

Nevertheless, it could partially be harnessed in the short run using peak-shaving on a [MW] scale, with relatively low volumes. At the same time other consortia actually already aim to produce green hydrogen based on offshore wind (Reuters Editorial, 2019). In the somewhat longer run this could become viable in the Netherlands as well (Wijk, 2019b). However, it would require a vast quantity to be at the scale needed to maintain the energy throughput function of the PoR. It further raises the interest in green hydrogen import, as well as the techno-economic feasibility.

2.2 Green hydrogen supply chains

Since it would require tremendous amounts of electricity to reach a substantial hydrogen production, locations with abundant renewable energy resources and thus relatively low production costs are preferable, when shipping does not add substantial costs. This could be for instance in wind rich regions (e.g. Patagonia) or regions that have plentiful solar resources (e.g. North Africa or the Middle East) (Heuser et al., 2019; Wijk, 2019a). It is for this reason that most of the studies investigate regions that have these characteristics or a combination of them.

Even though these global hydrogen trade links have not actually developed and effectuated yet, interest in academia has substantiated over the years. Several studies explored the feasibility of international hydrogen supply chains as well as what the most economical hydrogen carrier would be.

Moreover, some studies estimated the cost of hydrogen production. These studies range from a solely production oriented cost analysis to more comprehensive studies that also include the compression and shipping of hydrogen. In Scopus, a selection was made to understand what the most recent estimates are. The articles were found using the keywords: techno economic analysis hydrogen. Since the date is crucial for having up to date parameters, only articles published in 2018 and 2019 were selected.

Table 1 provides for a comparison of different studies on the cost of hydrogen production making use of renewable energy resources. Moreover, the size is given as this could foster economies of scale. It should be mentioned that even though these studies seem to be comparable, the assumptions vary substantially amongst them. The CE Delft study has been included since it was requested by the PoR at the time. It clearly shows how fast cost developments could be.

Table 1: This table provides for an overview of cost analysis conducted after 2018.

Study	Year	Includes	[MW]	Tech	Region	$[\$ \cdot kg^{-1}]$
CE Delft. (2017).H2 uit d.e.	2017	Production & transport	3.9	PV	Sohar, Oman	29.8
(Touili et al., 2018)	2018	Production	8	PV	Morocco	4.64
(Papadopoulos et al., 2018)	2018	Production	15 & 2	Wind&PV	Belgium	4-7
(Ayodele & Munda, 2019)	2019	Production	4.5	Wind	South Africa	1.4
(Heuser et al., 2019)	2019	Production & transport	95,000	Wind	Patagonia, Argentina	4.44
(Armijo & Philibert, 2020)	2019	Production	Ratios	Wind&PV	Chile, Argentina	1.9-2.3

Besides, it is important to put a figure on what transport would add to the cost of production and shipping. According to Niermann et al, from an economic perspective methanol has the highest potential over longer distances. The main reason is the relatively high energy density per volume as well as the low shipping costs. It is however dependent on the distance as well as other parameters (Niermann et al., 2019). Furthermore, it is crucial to understand that supply chain costs as a whole should be evaluated, not only looking at the costs of transportation.

It becomes clear that, except for the Patagonia study that is focused on wind as a renewable resource, there are no systems described in literature that are based on solar energy at the same scale (95 [GW]) as in the Patagonia study (Heuser et al., 2019). In 2002, the PoR acquired a 50% participation in the PoS in order to foster its international strategic connectivity (Van Den Bosch et al., 2011). From this perspective, given the favourable solar conditions for electricity production in combination with electrolysis in Sohar, it has been suggested to set up a (green) hydrogen value chain having its production in Sohar (Wijk, 2019b).

2.3 Local conditions Oman

The PoS is located in the far north in Oman. An illustration of the region is given in Figure 6. The PoS is located slightly north of Sohar, where the red indicator is the location of Fahud. It consists of two main industrial areas, where various industries are located. Among others, there is cement production, a refinery, a methanol plant with a capacity of 3,000 $[\mathrm{t} \cdot \mathrm{day}^{-1}]$ and an urea plant of 3,000 $[\mathrm{t} \cdot \mathrm{day}^{-1}]$. The refinery, methanol plant and the urea plant require hydrogen. The refinery consumes on average 295 $[\mathrm{t} \cdot \mathrm{day}^{-1}]$ of hydrogen for hydro-treatment and hydrocracking (Costa, 2019). The former in order to remove impurities from the crude oil, the latter to enhance residual oil into more valuable products (IEA, 2019).

The methanol is produced from hydrogen and CO_2. The hydrogen is produced by an SMR plant that uses natural gas. Since the methanol plant produces 3,000 $[\mathrm{t} \cdot \mathrm{day}^{-1}]$, the required amount of hydrogen could be derived making use of the chemical equation as well as the molar masses of methanol and H_2. The total amount of hydrogen required is 566.2 $[\mathrm{t} \cdot \mathrm{day}^{-1}]$ for the methanol plant only.

The urea plant has the same daily production of 3,000 $[\mathrm{t} \cdot \mathrm{day}^{-1}]$. Urea is produced from ammonia and CO_2. In turn, the ammonia is produced from hydrogen and nitrogen using the Haber-Bosch process. Therefore also the hydrogen demand from the urea plant could be derived using again the chemical equations and the molar masses. The total hydrogen demand for the urea plant is 302.1 $[\mathrm{t} \cdot \mathrm{day}^{-1}]$.

Figure 6: Overview of the region, the red marker indicates where Fahud is located, the PoS is very close north of Sohar.

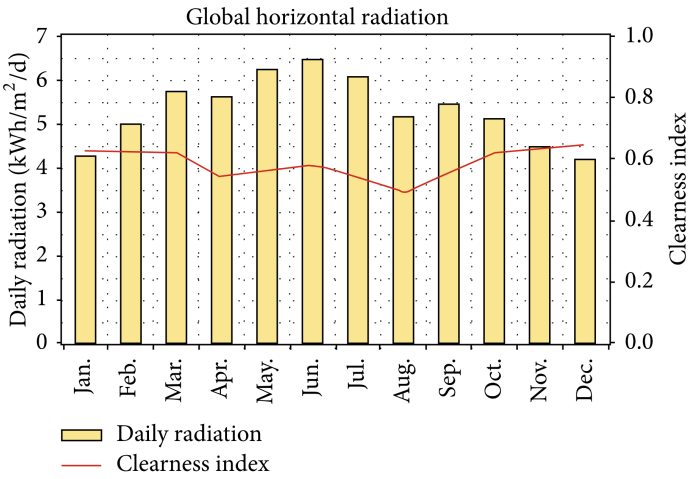

Figure 7: Global horizontal irradiance and clearness index monthly average for Sohar (Kazem et al., 2015).

Oman is rich in its solar resource. The average monthly global horizontal irradiance as well as the clearness index are provided in Figure 7. The capacity factors for fixed tilt solar pv systems are relatively high. Albadi et al. identified these capacity factors in different cities in Oman. In addition, the capacity factors are ranked and show that both Fahud and Sohar score relatively well with a capacity factor of about 0.19 for a fixed tilt system (Albadi et al., 2011). Figure 8 provides for this overview in capacity factors.

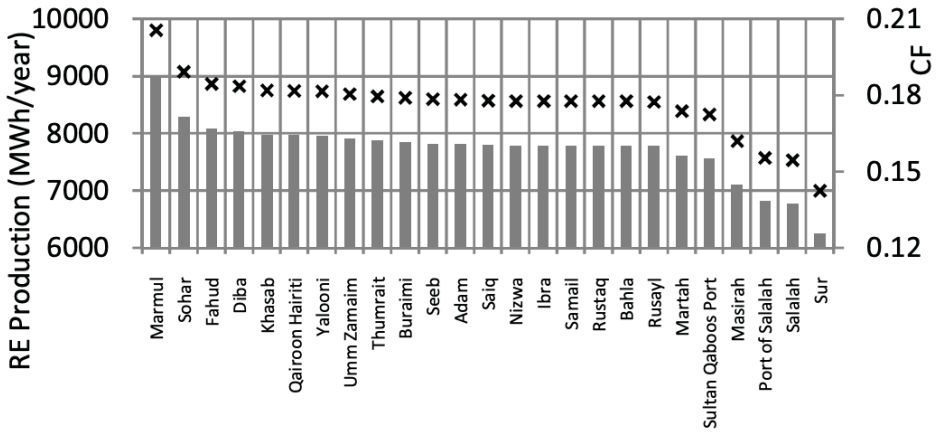

Figure 8: Fixed tilt solar pv capacity factors ranked for 25 cities in Oman. The energy produced should be ignored since it is system specific for the system studied by Albadi et al. (Albadi et al., 2011).

As solar pv requires relatively large areas, the Fahad Salt Basin has been identified as a potential suitable site for installing a large solar array (as a reference see Figures 6 and 17). It has the advantage of having moderate elevation differences as well as a high direct normal irradiance (see Figures 9a and 9b).

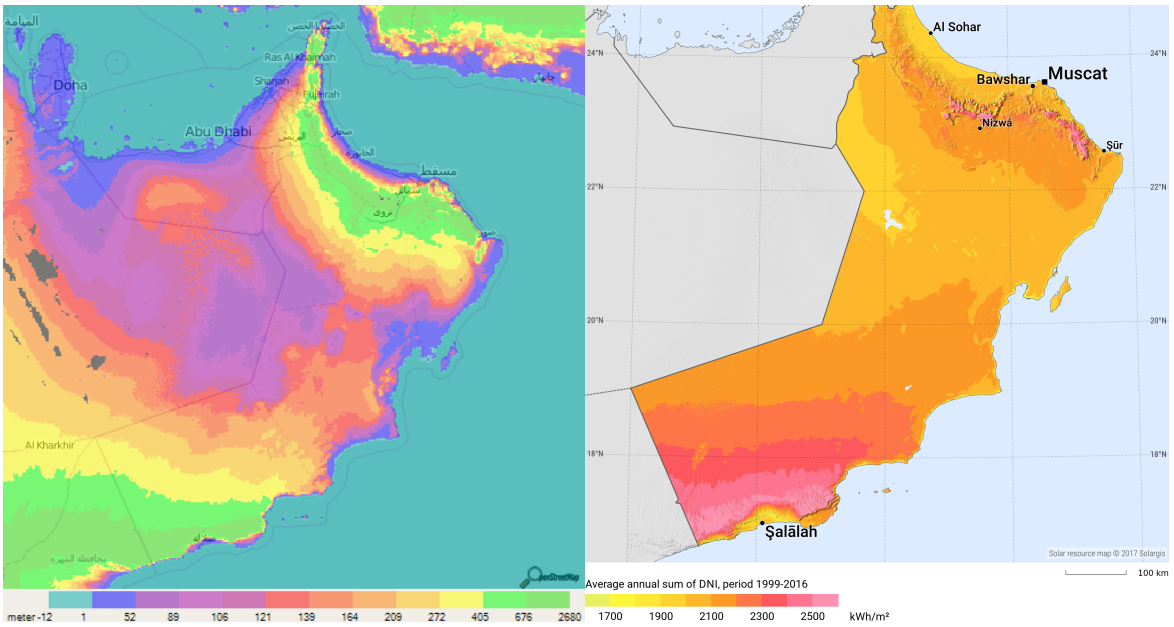

(a) Elevation level (Floodmap, 2019). (b) Direct normal irradiation (Albadi et al., 2011).

Figure 9: Both the elevation level as well as the average annual sum of the direct normal irradiation (Kamiya et al., 2015).

Currently the Fahud Salt Basin is under concessions for drilling fossil fuels mostly. Besides, there is an already existent corridor between the PoS and the salt basin, with natural gas pipelines that allow for potential synergies. This corridor could be used for the powerlines to provide transport electricity in subsequent stages in the supply chain, the permeate flow from the reverse osmosis units near the PoS and eventually the flow of oxygen that might help industries in the PoS region to become more efficient. Besides, the possibility might exist to create salt caverns that could overcome the variability in production when the solar pv output is zero. Moreover, the land cost could potentially be as low as 0.1 [$\$\cdot m^2$] (Costa, 2019).

2.4 Technology development

Obviously, not only the renewable resource availability is required to make green hydrogen supply chains feasible. Cost factors are crucial as well, costs of renewable energy technologies but for instance also costs of other stages of converting the electricity into hydrogen (electrolyzers). Besides, costs of storage, compression, pipelines, liquefaction and shipping should be carefully evaluated. Even though some of these technologies are relatively mature, others are less so. Each of these technologies will be evaluated in this Section in order to understand what technologies could be harnessed to set up a green hydrogen supply chain.

2.4.1 Renewable energy

Figure 10 allows for a comparison of LCOE values between four main renewable energy technologies. A first glance at this Figure suggests onshore wind as well as solar pv show the lowest LCOE values, which makes them favourable as it could also reduce the levelized cost of hydrogen). However, as onshore wind resources are limited in the region near the

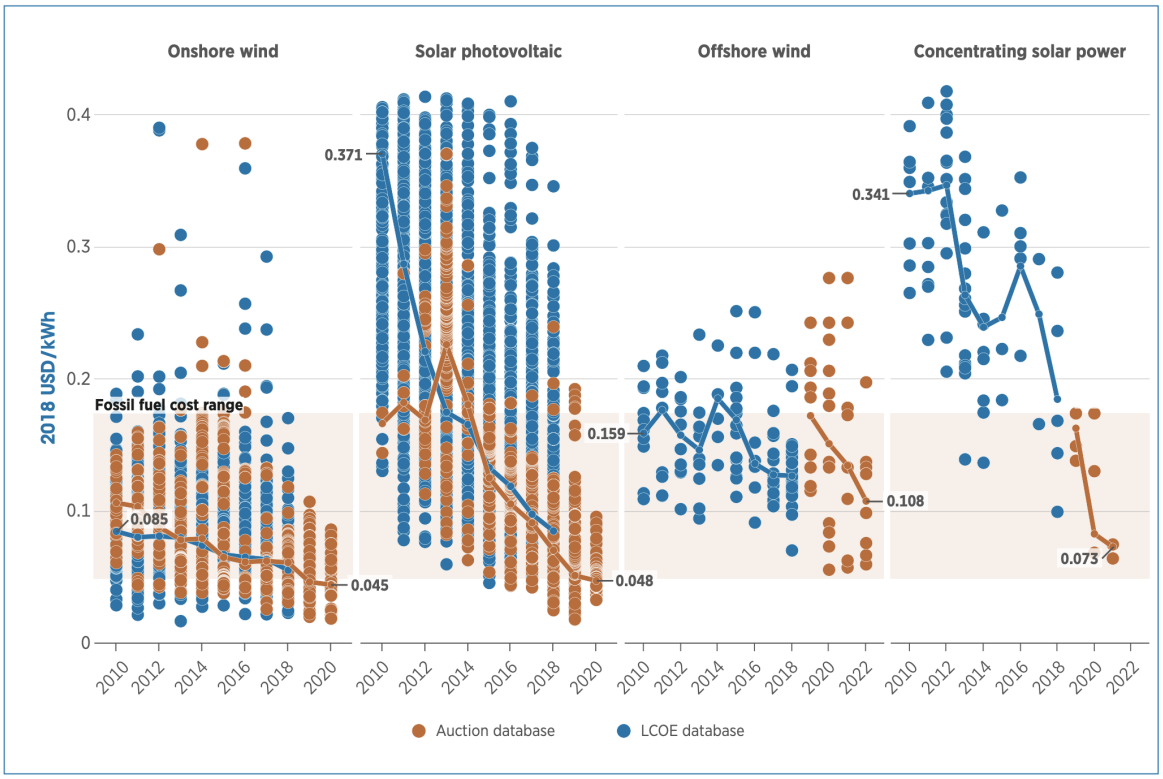

Figure 10: Cost declines for different LCOE factors of renewable energy technologies (IRENA, 2018).

PoS, only solar pv is considered (Atlas, 2019). Besides, at 2018 price levels, the Fraunhofer Institute argues that in regions with a high direct normal irradiation of 2000 [kWh $\cdot$ m^2], the LCOE of solar pv is lower than the LCOE of concentrated solar power (CSP) (Fraunhofer Institute, 2018).

2.4.2 Electrolyzer

There exist three main technology options for electrolyzers, that each has different characteristics. Fist of all, there exist alkaline electrolyzers (AEC) that are technologically mature and operate at low temperature. This type is typically a robust and cheaper option since no precious metals are used in the production. As a result, the $CAPEX$ is relatively low. The working principle is depicted in Figure 11a. It becomes visible that the hydrogen is produced at the cathode, the hydroxide flows through the diaphragm towards the anode where the oxide is produced. The water flows in opposite direction towards the cathode, where hydrogen is produced. The electrolyte is potassium hydroxide.

The second type is the polymer electrolyte membrane electrolyzers (PEMEC), has a higher power density and a high hydrogen purity, yet more complex and expensive alternative in comparison to the AEC. It has however the ability to easily switch up and down. At the same time, it has a smaller lifetime than the AEC type. The working principle of the PEMEC electorlyzer is depicted in Figure 11b, where the exchange through the membrane of hydrogen ions are passing through the membrane.

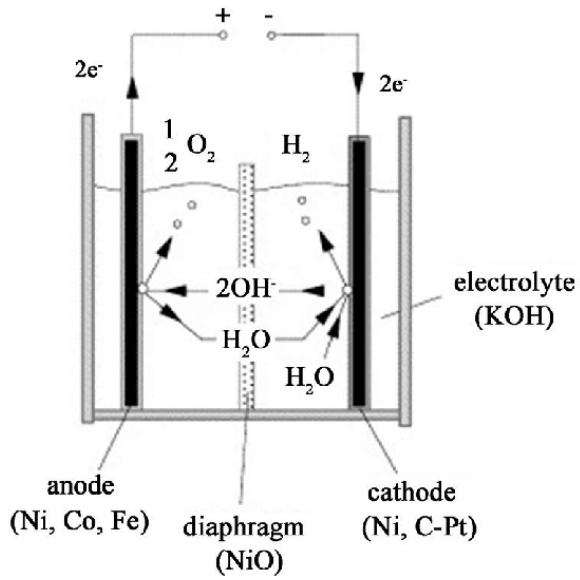

(a) Alkaline elctrolyzer (Shedid & Elshokary, 2015).

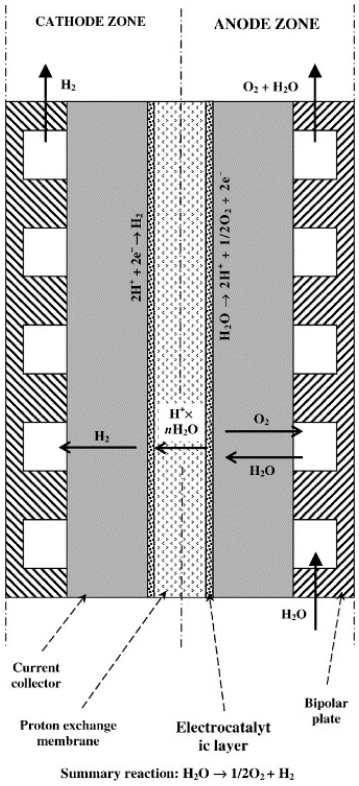

(b) PEM electrolyzer (Grigoriev et al., 2006).

Figure 11: Working principles of both the alkaline and PEM electrolyzer.

The third type is the solid oxide electrolysis cell (SOEC). Potentially it has a high electrical efficiency and relatively low material costs, but it is the least developed of the three alternative electrolyzers. Besides, it requires to be operated at high temperatures (Schmidt et al., 2017).

2.4.3 Stable electricity

Since there are a several elements in hydrogen supply chains that require a stable source of electricity in order to perform in a more energy and cost efficient manner (e.g. the liquefaction plant etc.), a stable supply of electricity is needed for these elements. There exist several options: electricity from the grid, a fossil based power generator, a CSP plant with thermal energy storage, a fuel cell system, or a battery system. However, since the set up of this supply chain is intended to be low carbon, only the CSP plant with thermal energy storage, the fuel cell and the battery system in combination with a local solar pv system is considered here.

The former option, using CSP as a stable supply for the liquefaction etc., is currently (2018 price levels) more expensive than the alternative of using solar pv in regions with a direct normal irradiance of 2000 $[\text{kWh} \cdot \text{m}^{-2} \cdot \text{year}^{-1}]$ (Fraunhofer Institute, 2018). It would also require a thermal energy storage system next to the CSP facility. Even though the battery

costs have to be added as well, the overall costs are assumed to be lower for a combination of a battery system with solar pv or a fuel cell.

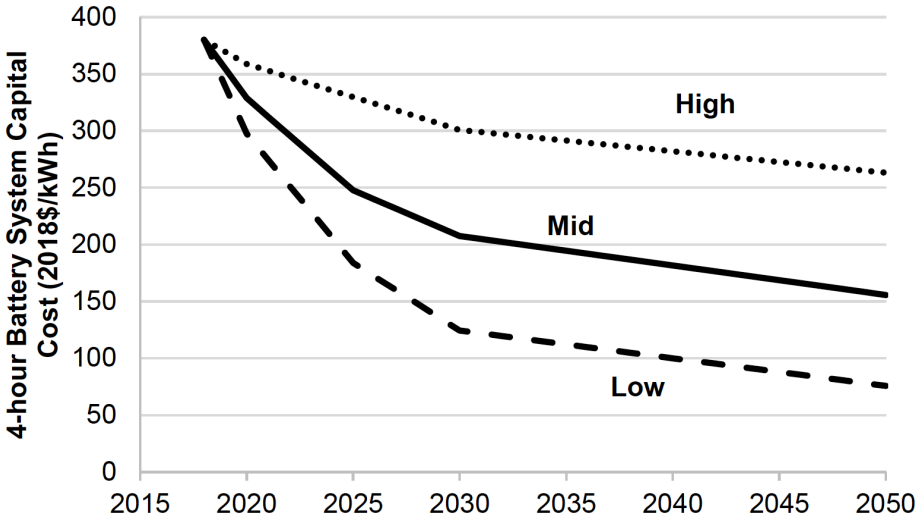

Figure 12: Cost projection 4-hour lithium-ion battery storage system, including costs for the complete system (Cole & Frazier, 2019).

The battery system would have to cover the time when the pv system is not operating. A commonly used battery technology is the lithium-ion battery. The National Renewable Energy Laboratory has made cost predictions for utility scale battery systems. The current low estimated costs for utility scale battery systems are 297 $[\$ \cdot \text{kWh}^{-1}]$ for a 4 hour utility scale battery storage system as projected in 2020. In Figure 12 the cost estimates for utility scale lithium ion batteries is depicted, projected by NREL (Cole & Frazier, 2019).

Typically, a debt of discharge of 80% is assumed and a round-trip efficiency of 85% (Cole & Frazier, 2019). A typical lifetime of lithium-ion batteries is 15 years, although it is heavily dependent on the debt of discharge. The land requirements for the battery are in 0.012 $[\text{m}^2 \cdot \text{kWh}^{-1}]$, the same footprint as the Megapack introduced by Tesla that requires three acres per [GWh] of storage (Tesla, 2019). Lastly, the fixed operational expenditure ($fixOPEX$) is 2.5% where the degradation of the battery system is overcome by this $fixOPEX$. It is important to note that these battery costs are [kWh] based, and have to be adjusted by the duration in order to become [kW] based, which would further increase costs (Cole & Frazier, 2019).

Fuel cells have seen substantial cost reductions as well. It is likely these costs will further drop with advances in manufacturing, economies of scale and R&D. The price of fuel cells is typically defined per [kW] (IEA, 2019). Proton exchange membrane fuel cells (PEMFC) are fuel cells that operate with a solid polymer electrolyte that allows protons passing through the electrolyte, while blocking the electrons. A PEMFC typically operates at a temperature between 353-373 [K]. An illustration is provided in Figure 13 (Mohan et al., 2019).

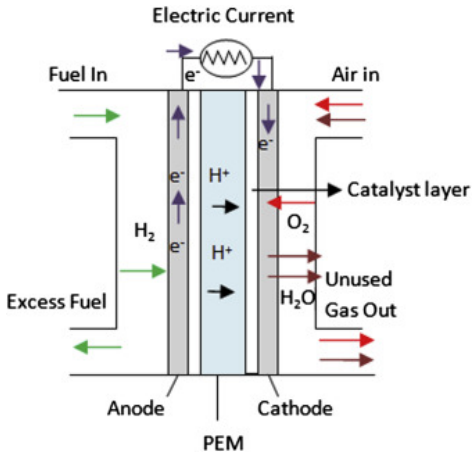

Figure 13: Illustration of the working principle of a PEMFC (Mohan et al., 2019).

Currently, the price of PEM fuel cells, which are predominantly used, is 230 [$·kW^{-1}], while in 2017 cost estimates of 40 [$·kW^{-1}] were predicted for 2020 (Satyapal, 2017; Bruce et al., 2018). These costs are however for transport applications. Utilisation of hydrogen for re-electrification in power plants shows higher costs (IEA, 2019). Bruce et al. show 568 [$·kW^{-1}] is reasonable for a [MW] scale PEMFC power plant in the best case scenario. Besides, in order to be competitive with a battery energy storage system in terms of *LCOE* coming from the power plant, a hydrogen price of about 1.6 [$ · kg^{-1}] or lower is needed. It depends on the capacity factor and the size of the power plant taken into account (Bruce et al., 2018).

2.4.4 Liquefaction

Liquefaction is a technology that has been around for quite some time and was initially developed for producing hydrogen in space applications. It concerns cooling down hydrogen to 20 [K] in order to make it liquid and thereby increase the volumetric energy density from around 0.089 [$kWh \cdot m^3$] at ambient conditions up to about 2,366 [$kWh \cdot m^3$] in a liquid state (Di Profio et al., 2009; Heuser et al., 2019). In Figure 14, a simplified schematic of hydrogen liquefaction process is provided.

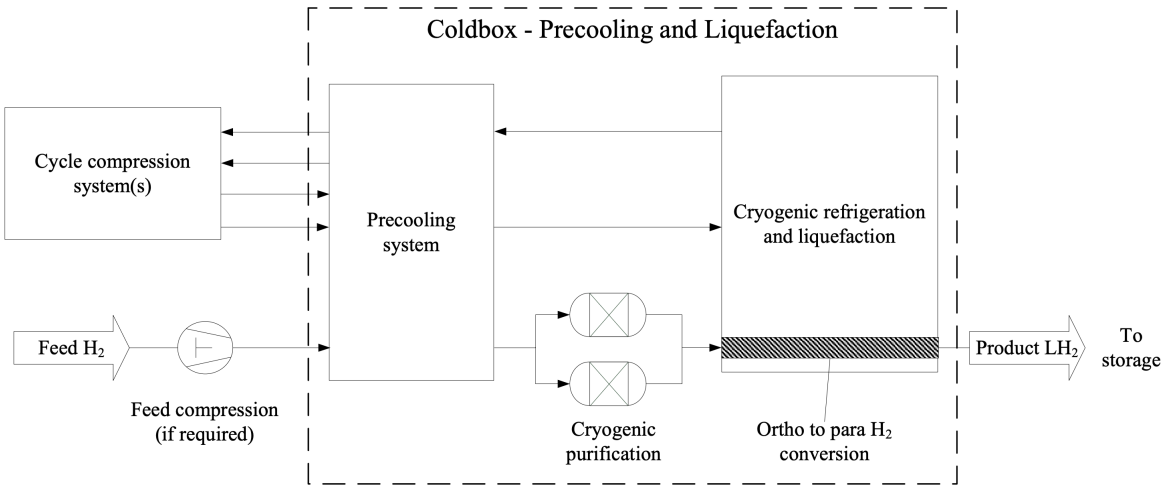

Figure 14: Simplified hydrogen liquefaction flowchart (U. F. Cardella, 2018).

There exist two main processes to liquefy hydrogen: the Reversed Helium Brayton Cycle and the Claude Cycle. Both concern precooling of hydrogen with liquid nitrogen. However, the second step involves in the former case a helium cooling cycle and ultimately a Joule Thomson valve where it is cooled from 30 to 20 [K]. In liquefaction, the refrigeration is effectuated by the decrease in pressure that causes a drop in temperature. The Joule Thomson valve is a simple system that provides for this cooling (U. F. Cardella, 2018). The latter process (Claude cycle) uses instead of the helium cooling cycle recycle compressors.

In Figure 15, a comparison is provided to evaluate the two main liquefaciton technologies. The prime difference is the trade-off betweeen $CAPEX$ and $OPEX$ of the two processes. Generally, the Reversed Helium Brayton Cycle requires lower $CAPEX$ costs and higher $OPEX$ costs in comparison to the Claude Cycle. Correspondingly, bigger capacity plants have both a lower specific $CAPEX$ and $OPEX$ per unit, while bigger investments enable a lower $OPEX$. Both developments are also visible in Figure 16.

According to the company Linde, a specific energy consumption close to or below 6 [$kWh \cdot kg^{-1}$] hydrogen is within reach for installations around the 100 [tpd]. A cost reduction of about 70% would be possible (U. Cardella, 2019). This is already close to the thermodynamic ideal work. The thermodynamic ideal work depends on the input pressure, the ratio between ortho and para hydrogen (different spin of the hydrogen nuclei) and the input temperature. The thermodynamic ideal work from 1.01 [bar] gaseous hydrogen at 300 [K] to liquid hydrogen at the same pressure but at 20 [K], is 3.3 [$kWh \cdot kg^{-1}$] (Syed et al., 1998).

	Current Technology		***Short Term Future***	***Medium Term Future***
Liquefaction Capacity, tpd	**<3**	**2 - 15**	**15 - 30**	**<200**
Main Rerigeratin Cycle	Brayton	Claude	Claude	Claude
Refrigeration Medium	Helium	Hydrogen	Hydrogen	Hydrogen
Pre-cooling Cycle	LN_2	LN_2	Chiller & N2 Cycle	N2 / Mixed Refrigerant Cycle
Compressor Type	Oil Flooded Screw	Piston	Piston	Piston
Feed Pressure (Bar)	10 - 15	15 - 20	20 - 25	> 20
Specific Power (kWh / kg H2 (Including feed gas compression & precooling)	**13,4 - 12.3**	**12,7 - 10,8**	**10,8 - 7,7**	**9 - 7,5**
Operating Cost (OPEX)	Highest	Low	Lower	Lowest
Investment Cost (CAPEX)	Low	Medium	Higher	Highest

Figure 15: Comparison between liquefaction technologies (NCE, 2019).

The inlet pressure for the IDEALHY study is 82 [bar] and the specific energy consumption is visible in Figure 16. The exergy efficiency of the IDEALHY liquefaction installation is 42% (U. Cardella et al., 2017). The difference between the specific energy consumption per [kg] hydrogen for Linde and IDEALHY is due to a higher feed pressure as well as using a Mixed Refrigerant Joule Thomson Cycle (U. F. Cardella, 2018). The Mixed Refrigerant Joule Thomson Cycle enables a more extensive range of condensation and evaporation temperatures, while also enabling a lower energy consumption.

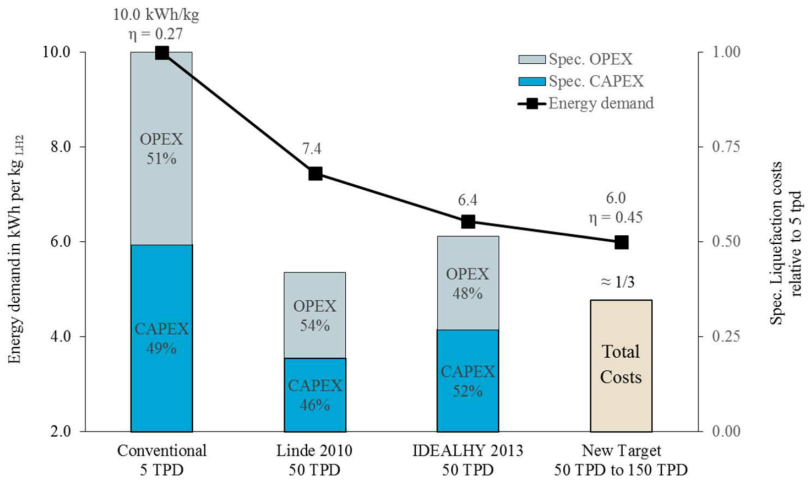

Figure 16: Development of both energy demand and costs of liquefiers (U. Cardella et al., 2017).

2.4.5 Hydrogen storage

As said before, some supply chain stages benefit from a stable flow by becoming more energy efficient (Stolzenburg & Mubbala, 2013). Other stages simply require a stable source for shipping. Furthermore, specific investment costs for $CAPEX$ decrease. Several options exist regarding hydrogen storage. Since hydrogen has a low energy density at low pressure, either pressurizing or binding it to other components has been suggested. However, these different storage methods significantly differ in costs and scalability. Both pressurized hydrogen in tubes and liquid organic hydrogen compounds (LOHC) have significantly higher specific $CAPEX$ costs in comparison to salt cavern storage and liquid storage (Reuß et al., 2017). Therefore, these last two technologies will be elaborated upon.

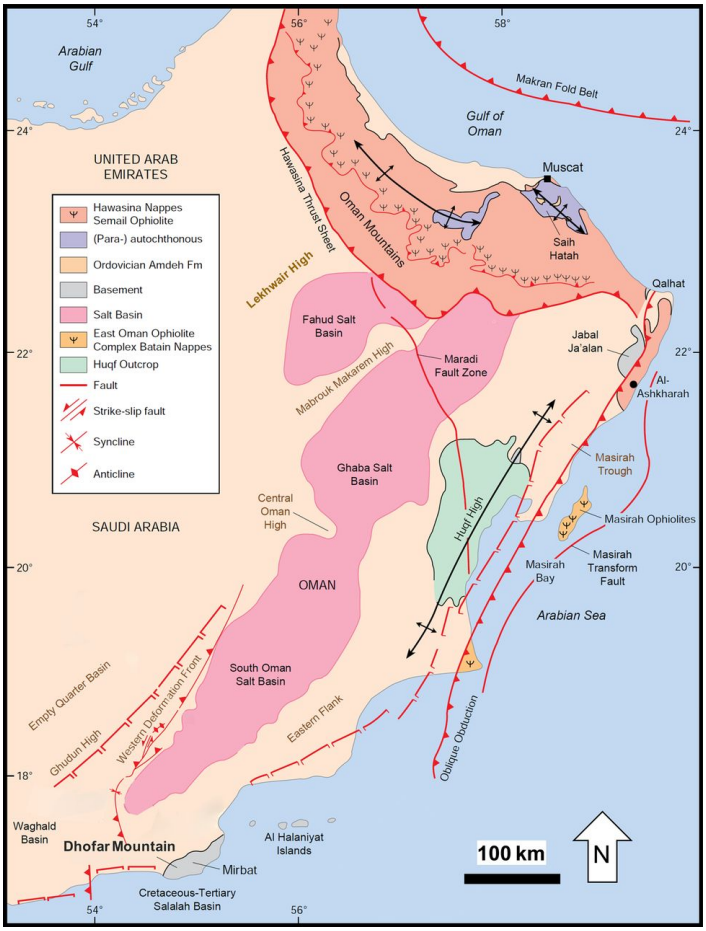

Figure 17: Overview of the salt basins in the region (Al-Kindi & Richard, 2014).

First of all, salt cavern storage will be evaluated. Reuss et al. compared storage transport combinations, and showed the lowest costs are achieved for distances over 200 [km] and daily throughput of over 20 [t] hydrogen in the case of cavern storage and a gaseous hydrogen pipeline (Reuß et al., 2017). Salt caverns are human made cavities in salt deposits that are very tight in nature, which makes them feasible for gas storage. Historically they have been used for natural gas storage, and they are typically close to former or still existing fossil fuel resources. Similarly, for instance in Teesside (UK) and Texas (US) salt caverns are already used for hydrogen storage and are part of hydrogen infrastructures (Crotogino et al., 2010).

They require a relatively small footprint and have low specific investment costs. Besides, they allow large scale storage at pressures up to 200 [bar] (Crotogino et al., 2010). The lifetime of salt caverns is considerably long and there is quite some built up experience from a geological perspective. Perhaps most importantly, they allow for daily variation of storage volumes and therefore are particularly well suited for storing hydrogen produced with renewable energy resources (Michalski et al., 2017).

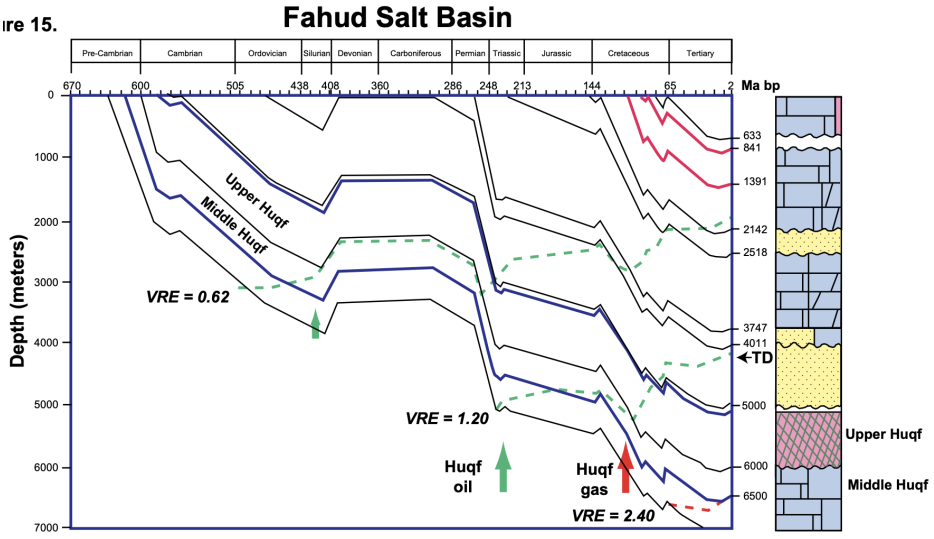

Figure 18: Cross section Fahud Salt Basin, the Upper Huqf is a salt layer (Pollastro, 1999).

However, not all salt caverns are feasible. A thick layer of about 200 [m] is required and the depth at which the salt caverns are constructed should not be deeper than about 2,000 [m]. More precisely, the top of the salt layer should be in the range of 500 and 2,000 [m]. Furthermore, the brine that is created due to construction should be disposed in a environmentally sound manner (Michalski et al., 2017). In addition, an investment has to be made in cushion gas that remains in the cavern to prevent water and other substances leaking in the salt cavern (Tarkowski, 2019). A first impression of the lithosphere in Oman shows that it has several salt deposits that are shown in Figure 17. Since depth and width are crucial for evaluating whether hydrogen storage in salt caverns is feasible, Figure 18 depicts the cross section of the Fahud Salt Basin. According to this cross section, the Fahud Salt Basin, that is relatively close to the Port of Sohar (about 200 [km]) could be feasible to construct a salt cavern in this region. The depth is in the admissible region.

Secondly, liquid storage is evaluated. Liquid sotrage has been around for decades and was initially used for space applications. It is a relatively well developed storage option. A disadvantage of liquid storage is the inability to ensure perfect insulation. For this reason boil-off gas is inevitable. Hence, in order to minimize the surface area with respect to the volume, typically large spheres are preferable. Small spheres of 50 [m^3] have boil-off rates of about 0.4% whereas larger spheres have boil-off rates of smaller than 0.03% per day (USdrive, 2017). Currently, the biggest liquid hydrogen storage is at NASA and has a volume of 3,800 [m^3]. For comparison, different sized spheres are depicted in Figure 19. The liquid hydrogen storage currently in development in the supply chain between Australia and Japan has a volume of 2,500 [m^3] (Weterings, 2019).

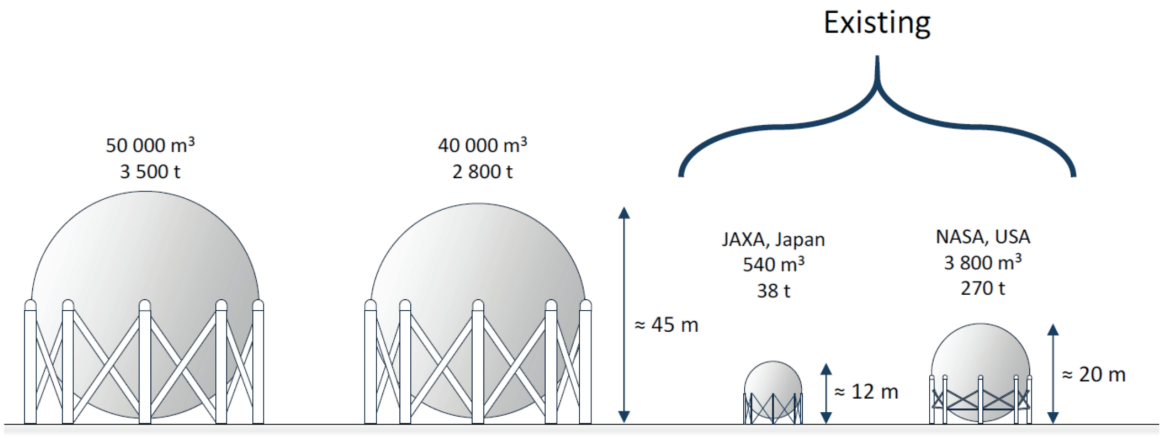

Figure 19: Cryogenic hydrogen storage (NCE, 2019).

2.4.6 Hydrogen shipping

There exist roughly three different modes of shipping hydrogen. The first mode is shipping hydrogen in liquid form, using liquefaction. Hydrogen has to be liquefied, as mentioned before in more detail. Even though transportation of hydrogen in gaseous state via pipelines and trucks is a mature technology, international shipping is not well developed (IEA, 2019). Nevertheless, the first hydrogen carrier conceptual designs have been drawn by Kawasaki.

The small-scale LH2 carrier has a capacity of 2,500 [m^3] and still has diesel propulsion. The large-scale 160,000 [m^3] LH2 carrier is propelled by the boil-off gas created due to imperfect insulation of the spheres. Four spherical tanks are aboard of this large ship, that have a diameter of 45 [m] (Kamiya et al., 2015). Both ships are depicted in Figure 20. In addition, in December 2019 the first actual liquid hydrogen ship by Kawasaki has been launched in Japan that has a capacity of 1,250 [m^3] of hydrogen, and has diesel powered propulsion (Harding, 2019).

Liquid hydrogen is comparable to LNG, especially the mode of shipping as well as the need for insulation and the boil-off. The characteristics are listed in Table 2. In LNG shipping, historically the boil-off gas was used as the propulsion fuel, making use of steam turbines. However, as the ship size increased and simultaneously the need for efficiency, dual fuel diesel electric has been developed that is able to use both boil-off gas as well as diesel fuel. Nowadays, the trend towards complete re-liquefaction aboard the ship is followed, no longer making use of the boil-off as a propulsion fuel for the ship but instead re-liquefying the boil-off and using for example diesel fuel (Tu, 2019).

Table 2: Comparison between LH2 and LNG (Kamiya et al., 2015).

	LH2	LNG
Liquid density [$kg \cdot m^{-3}$]	70.8	442.5
Gas density [$kg \cdot m^{-3}$]	1.34	1.82
Boiling point [K]	20.3	111

(a) Small hydrogen carrier design (b) Large hydrogen carrier design

Figure 20: Conceptual designs proposed by Kawasaki industries (Kamiya et al., 2015).

The second mode is by means of liquid organic hydrogen carriers (LOHC). It is a family of different organic compounds that could be hydrogenated for transport and dehydrogenated at the point of consumption (e.g. toluene, methanol). It has the advantage of having similar characteristics as international fossil fuel transport, therefore encountering few barriers for adaptation. Dehydrogenating typically requires heat, which could either be produced by burning the hydrogen, or by using waste heat. The latter is the preferred option as it would improve the efficiency. An illustration of a LOHC supply chain is given in Figure 21. It becomes clear from the Figure that the carrier has to be shipped back, which is a disadvantage of using these carriers (IEA, 2019).

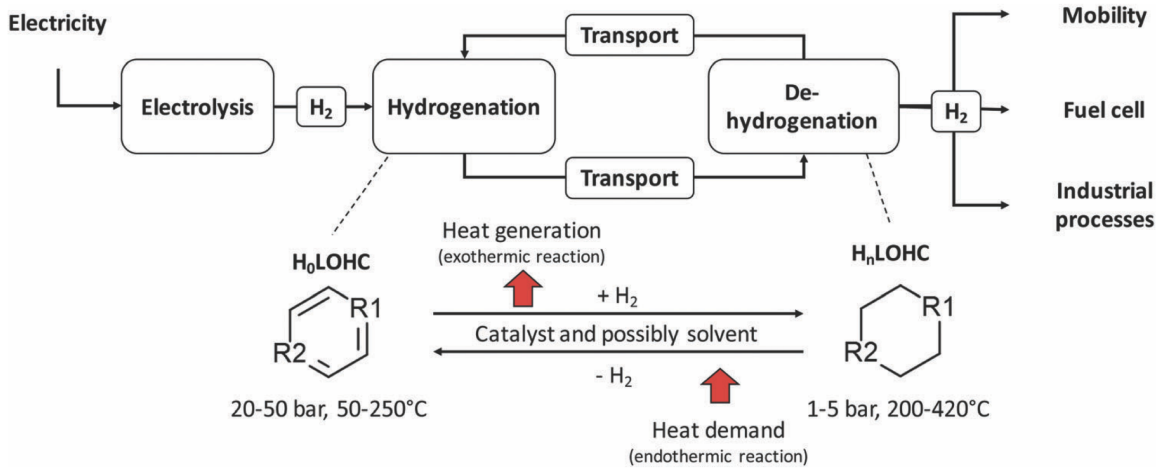

Figure 21: Conceptual LOHC supply chain (H_0 is unloaded and H_n is loaded) (Niermann et al., 2019).

The third hydrogen carrier is ammonia, which already is a major hydrogen market as indicated by Figure 1. It fits well into existing international trade links and the technology is mature. As the dehydrogenation of ammonia requires a substantial amount of heat, it again would benefit from the availability of waste heat (IEA, 2019).

2.5 Capital costs

Renewable energy technologies are more capital intensive than their fossil counterparts, while $OPEX$ costs are typically lower (Best, 2017). As a result, the levelized costs of electricity or ultimately hydrogen is sensitive to the weighted average cost of capital ($WACC$) values, the discount rate used to discount future cash flows to present value. A representative $WACC$ for Oman would be about 7%, since this factor is proposed by Oman to evaluate renewable energy projects in the region (Costa, 2019). However, more recent numbers of the $WACC$ in renewable energy projects show lower values in the order of magnitude close to 1.6% $WACC$ (Bachner et al., 2019). These $WACC$ rates are in fact lower in developed countries. Even within countries there is heterogeneity in the $WACC$ rates that are being used. Recent research shows also lower rates for international solar pv auctions (Steffen, 2019). This would significantly affect the ultimate costs of hydrogen production. An illustration of perceived $WACC$ rates in solar pv is provided in Figure 22.

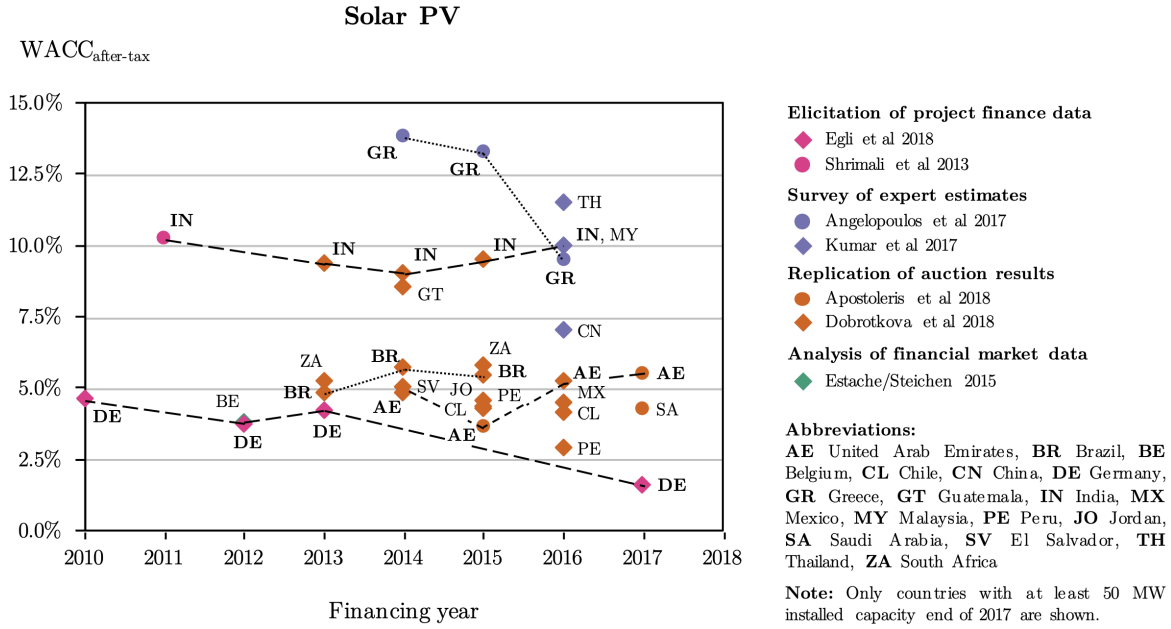

Figure 22: Overview of different $WACC$ rates (Steffen, 2019).

3 Methodology

In this Chapter, the methodology will be explained. As described in the introduction, this part of the thesis will focus on the Sohar side of the supply chain and will be a techno-economic analysis. First of all, a Section will focus on where and for what purposes techno-economic analyses are used. Secondly, an overview of the system will be provided. Thirdly, the different elements of the system will be described as cost models. Fourthly, these cost models will be explained in detail to understand how these elements contribute to the price of green hydrogen production in Sohar. Fifthly, the combination of each of these factors will be synthesized in a comprehensive model to ultimately derive a cost factor in $[\$ \cdot \mathrm{kg}^{-1}]$ of hydrogen produced. Lastly, the sensitivity of the different parameters (e.g. cost of solar pv) will be analyzed to understand what future price developments would mean for the price of hydrogen over the supply chain.

3.1 Research approach

A techno-economic analysis (TEA) is an analysis that evaluates the technical and economical performance of a product, service or system. The methodology is a tool to assess the economic feasibility, the future cash flows, the likelihood of the spread of a certain technology as well as the technological quality (Lauer, 2008). The cost assessment of the system studied includes the capital expenditure $CAPEX$, the fixed operational expenditure $fixOPEX$ as well as the variable operational expenditure $varOPEX$. In literature, there exist different methods. For this research, the annuity method is chosen, where the investment costs are spread over the project lifetime. It is a commonly applied method in Europe, especially for preliminary project evaluations. Besides, it is aligned with previous studies on the techno-economic analysis of a hydrogen supply chain (Heuser et al., 2019). Furthermore, it typically includes a sensitivity analysis in order to evaluate what the effect of changing a single parameter would be on the final result (Lauer, 2008).

3.2 System design

The system design characteristics are the following. First and foremost, the conceptual supply chain is partly located on the Fahud Salt Basin and partly in the PoS. The Fahud Salt Basin has relatively even elevation, is currently already under concession for oil drilling and there is already a corridor between Fahud and Sohar for fossil fuel transport (Floodmap, 2019; Costa, 2019). The supply chain is solely based on renewable resources, primarily solar pv and partly CSP. As a consequence, the capacity factor of the electricity production is rather small.

The solar pv system will have a capacity of 100 [GW], which should be approximately enough to produce hydrogen to cover the forecasted demand in Zuid Holland of 2.4 [Mt] as stated by Wijk et al. (Wijk, 2019b). Furthermore, a similar sized system is also the starting point in the analysis of a wind based green hydrogen supply chain conducted by (Heuser et al., 2019).

There are a several elements in the supply chain that benefit from a stable operation (e.g. liquefaction) by becoming more energy efficient, but more importantly by lowering the specific $CAPEX$ of each cost factor (more operating hours means lower $CAPEX$ per operating

hour). The design principles are based on this characteristic. The part of the supply chain that is located on the Fahud Salt basin will be variable due to a low capacity factor of the solar pv system. Hydrogen is produced only when electricity is available from the solar pv system, hence compressors at this side of the supply chain do not need to compress when no hydrogen is produced. Consequently, both electricity as well as hydrogen are variable. The variability will be covered by means of hydrogen storage.

After the hydrogen storage, both hydrogen and electricity will operate at base load. Hence, from the pipeline onwards, a stable stream of hydrogen will be transported towards the PoS. Since the supply chain elements after the pipeline operate mostly at nominal conditions, they will need base load electricity. The base load electricity is provided to the liquefaction plant and the liquid hydrogen pump by a subsystem.

3.3 System boundaries

The TEA includes various parameters that are relevant for the project, but before defining these parameters, it is important to set the scope of this analysis. Figure 23 depicts a flowchart and allows for a better understanding of the different processes that are involved. The supply chain elements that are indicated by a green color represent the stages that are located on the Fahud Salt Basin and the PoS. The boundaries in the flowchart indicate that the supply chain starts on the Fahud Salt Basin with solar pv and ends at the Port of Rotterdam as a kilogram of liquid hydrogen received, without any further handling costs considered here.

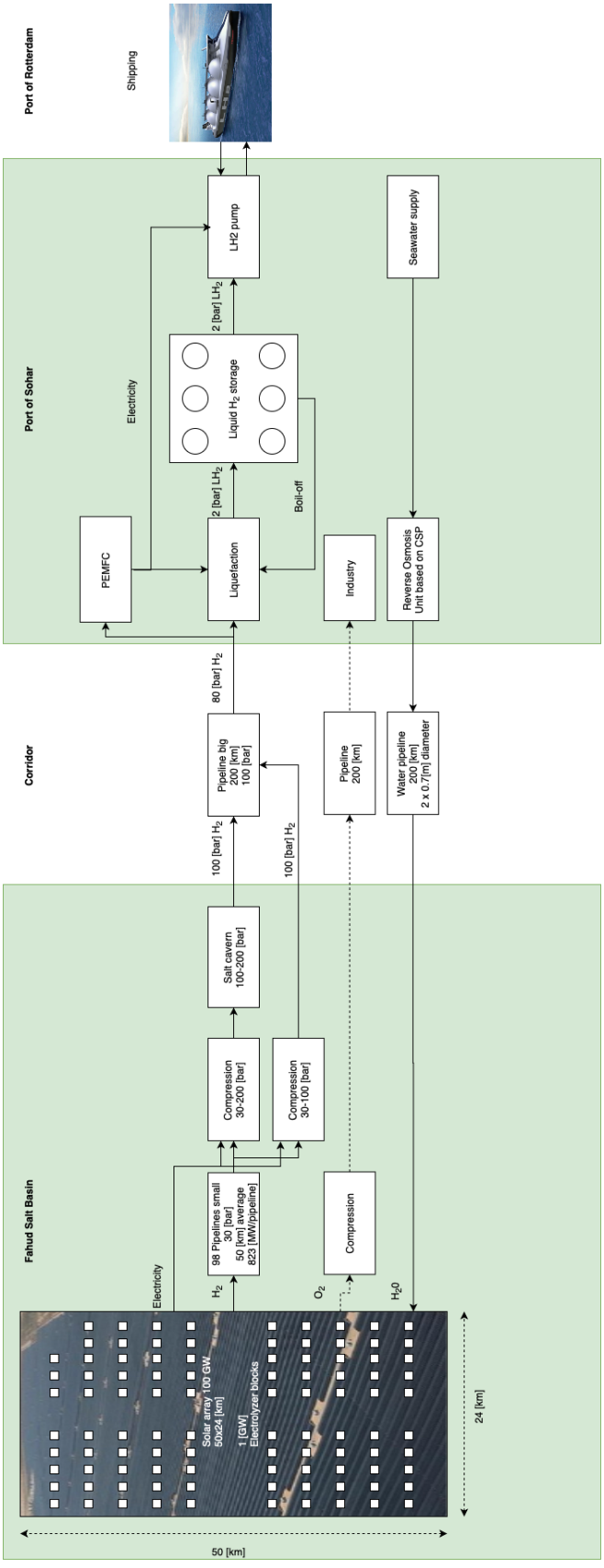

Figure 23: Flowchart of the processes that are considered in part 1. The white dots in the pv system indicate the [GW] electrolyzer blocks, from where the small pipelines transport the hydrogen towards the salt cavern storage. The oxygen is indicated with a dotted line, since it is not included in the cost model.

3.4 Cost model

In this Section, an overview of the different elements that contribute to the price of hydrogen is provided. The Spyder software is used in order to set up the model in the Python language. The cost model is adapted from the study of Reuss in combination with the study of Heuser (Heuser et al., 2019; Reuß et al., 2017). Moreover, the levelized cost of electricity $LCOE$ of solar energy is estimated, since this would have an influence on the price per [kg] of hydrogen produced in the system. Furthermore, all the cost factors are converted into USD, with a conversion rate of 1.1 [$/€]. Importantly, cost factors assumed for each supply chain element are current costs and chosen as recent as possible. No inflation corrections are conducted.

First of all, a several formulas are introduced that are adapted from Reuss (Reuß et al., 2017). The total amount of invested capital for each element is calculated based on Equation 1. This Equation is a scaling function that allows for a decrease in specific investment costs when the system is scaled up. Besides, it allows for making all the cost factors congruent.

$$Invest_{total}(\$) = Invest_{base} * \frac{Capacity}{Invest_{compare}}^{Invest_{scale}} \tag{1}$$

Moreover, the factor f_{prod} is used to compensate for cascading effects in the supply chain, since in some echelons the capacity factor is small (Reuß et al., 2017). The f_{prod} is applied to the compressors and the salt cavern only as every stage after the salt cavern works at base load (see Subsection 3.2). The FLH is calculated from a multiplication of the capacity factor of the solar pv system times the number of hours per year. Therefore, using Equation 2 the f_{prod} would be 5.3.

$$f_{prod} = \frac{8760}{FLH} \tag{2}$$

For each system element, the $CAPEX$, $fixOPEX$ and $varOPEX$ are calculated, making use of Equations 1,2,3,4,5.6 and 7.

$$Capacity = Capacity_{nominal} * f_{prod} \tag{3}$$

Since Oman is not listed in the $WACC$ study by Steffen, Saudi Arabia is chosen as a proxy. The markup to the LIBOR rate is found to be 2.5 % (Steffen, 2019). With the current LIBOR of 2% (2019), the after-tax WACC is taken to be 4.5% (Macrotrends, 2019).

The annuity is calculated using Equation 4. It enables adjusting for different lifetimes of each cost factor.

$$Annuity = \frac{(1 + WACC)^n * WACC}{(1 + WACC)^n - 1} \tag{4}$$

In Equation 5, the capital expenditure is calculated per unit of throughput, hence per [kg] of hydrogen produced.

$$CAPEX(\$/kg) = \frac{Invest_{total} * Annuity}{\text{throughput}} \tag{5}$$

The total land requirements are found by Equation 6, but is only conducted for land demanding supply chain elements: reverse osmosis, pv system, electrolyzer, salt cavern storage, fuel cell and liquid storage.

$$Land_{total}(\mathrm{m_2}) = Land_{base} * \frac{Capacity}{Invest_{compare}} \tag{6}$$

The fixed operational expenditure is defined as the operation and maintenance (OM) costs per [kg] of hydrogen, where the OM is a percentage of the total invested capital for that system element (see Equation 7). Besides, the land-lease costs are added to the $fixOPEX$ by multiplying the minimum total required land of each element with the land-lease costs of 0.1 [$\$ \cdot \mathrm{m}^{-2}$] (Costa, 2019). The overproduction factor f_{prod} is again only used for the compressors and the salt cavern.

$$fixOPEX(\$/kg) = \frac{Invest_{total} * OM * + Cost_{landlease} * \mathrm{Land}_{total}}{throughput_{nominal} * f_{prod}} \tag{7}$$

Finally, for each system element the total capital expenditure is calculated making use of Equation 8, where $varOPEX$ is a specific operational expenditure (e.g. water, electricity or hydrogen). The $varOPEX$ is left out of Equation 8 since the costs for either producing the electricity or the hydrogen are already incurred at other supply chain elements, which is different from approaches such as the one proposed by Heuser et al. (Heuser et al., 2019). This translates into a cost per unit of hydrogen for each supply chain element.

$$TOTEX(\$/kg) = CAPEX + fixOPEX \tag{8}$$

3.4.1 Reverse osmosis

The electrolyzer requires ideally 9 [kg] of water for every [kg] of hydrogen. The average precipitation in Oman is 125 [mm] (Worldbank, 2019). Since the fresh water availability is limited in Oman, desalinated water and the associated price should be included in the techno-economic analysis as well. Reverse osmosis is a technology that could be harnessed.

According to Laissaoui et al., at a scale of about 12 [Mt] of water production, a levelized cost of water of about 0.83 [$\$ \cdot \mathrm{m}^{-3}$] could be achieved, making use of a CSP system with thermal energy storage, since it achieves the lowest costs per [m^3] of water (Laissaoui et al., 2018). This would be a competitive price with the fossil based alternative, which has a levelized cost of water ranging between 0.60–1.90 [€$\cdot \mathrm{m}^{-3}$] (Laissaoui et al., 2018). The system proposed by Laissaoui et al. is depicted in Figure 24. It includes a 14 hour thermal energy storage system, which therefore operates at 72% of the nominal capacity. Furthermore, the base system requires 146,313 [m^2] for the solar field area (Laissaoui et al., 2018).

The actual reverse osmosis unit operates as a whole unit. It has a daily production of 35,000 [m^3] permeate water flow. It has a recovery rate of 42% and includes a pressure exchanger

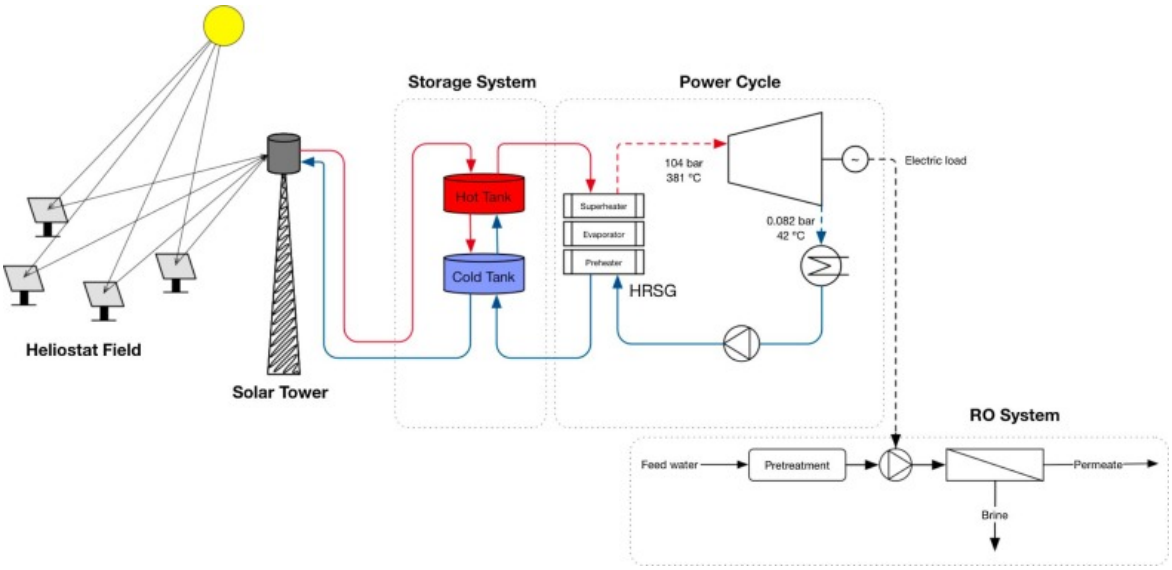

Figure 24: The combination of CSP and RO.

(PEX). Using Equations 9 and 10 it requires a feed flow of 83,333 [m^3]. Since the feed flow is the addition of the discharge brine flow plus the fresh water flow, the discharge brine flow is 48,333 [m^3] per day for the base system. The system is depicted in Figure 25 (Laissaoui et al., 2018). Finally, the brine is disposed in evaporative ponds, an approach that is common practice in Oman (Ahmed et al., 2001).

$$M_f(\mathrm{m}^3/\mathrm{day}) = \frac{M_d}{RR} \tag{9}$$

$$M_b(\mathrm{m}^3/\mathrm{day}) = M_f - M_d \tag{10}$$

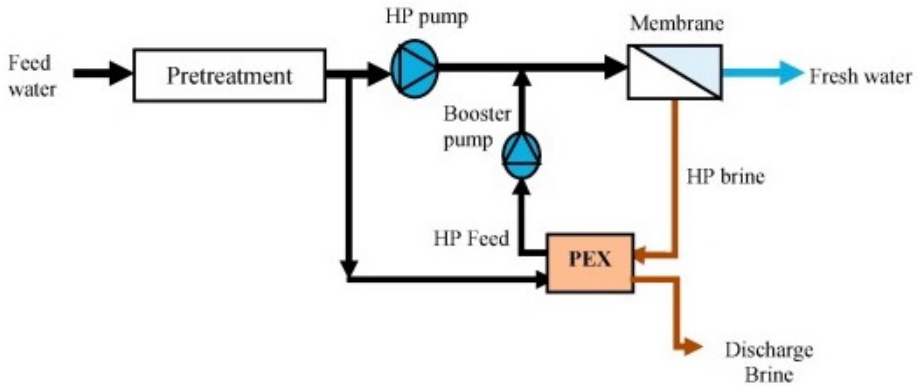

Figure 25: More detailed overview of the reverse osmosis unit, where a high pressure [HP] feed is fed back to the membranes.

In order to include to costs of the water supply, a sustainable water supply is chosen, based on a stand alone concentrated solar power (CSP). According to laissaoui et al., a system with a permeate flow of about 35,000 [$m^3 \cdot day^{-1}$] costs about 11 million USD, which is the

annual capital costs including the OM and is already annualized. This means that, since the $WACC$ is not disclosed in this study, the depreciation period is calculated as such to make the annuity zero. As a result, the annual capital cost per system is incurred every year. This base system is scaled to meet the water requirements of the electrolyzer. Lastly, it is assumed that the water has the right quality to be used in the electrolyzer, even though demineralized water would be necessary.

3.4.2 Water pipeline

The reverse osmosis system is located in the PoS. As a result, the permeate flow has to be transported towards the electrolyzers at the Fahud Salt Basin. As a result, the minimum water consumption could be derived from the hydrogen produced, which is scaled to $[m^3 \cdot day^{-1}]$. According to experts at KWR, two pipelines of 0.7 [m] diameter each would be feasible for a throughput of 85 thousand $[m^3]$ of water per day (Huiting & Vreeburg, 2020).

Two pipelines are proposed, as one could serve as a backup in case of a failure of the first pipeline. The pressure could simply be increased in either pipeline. The cost of the water pipeline from the PoS towards the Fahud Salt basin are assumed the following. Typical prices of large water pipelines of 0.7 [m] diameter are 550 $[\$ \cdot m^{-1}]$. Therefore, two pipelines would cost 1.1 million $[\$ \cdot km^{-1}]$ (Huiting & Vreeburg, 2020). The lifetime is assumed to be 40 years, the OM 1%. The length is the same as the hydrogen pipeline, which is 200 [km] from the PoS to the Fahud Salt Basin. A water buffer might be needed as well, but these costs are neglected since they would not add substantial costs.

3.4.3 PV array

In this Section, the methodology to assess the costs of the PV system will be analyzed. The pv array is directly linked to the electrolyzers in blocks of 1 [GW]. These blocks consist of rows of pv modules, facing the south. The optimal tilt angle for Oman is considered to be 25 degrees (Jacobson & Jadhav, 2018). A fixed tilt system is chosen, since it is the least capital intensive system. Besides, it is also used in the biggest solar pv plant in the world of 2 [GW], that will act as a blueprint for the pv array design (Verdict Media, 2020).

The spacing between the rows of modules is described by Equation 11. Furthermore, each of the variables are depicted in Figure 26. In this Equation, d is the distance between the two rows of pv modules, w is the width of the modules, h is the height of the modules, β and γ are the tilt and the shadow angle respectively.

$$d(m) = \frac{w * sin(180 - (\beta + \gamma))}{sin(\gamma)} \tag{11}$$

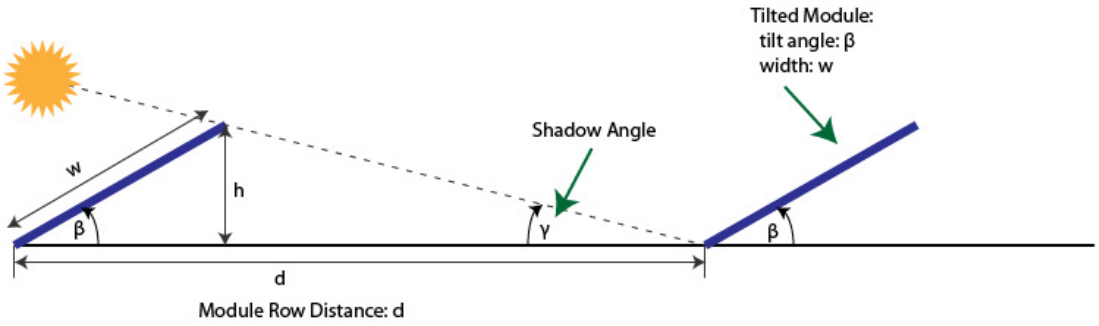

Figure 26: Schematic figure to find minimum spacing between rows of pv modules (Rhino Energy, 2016).

Generally, as a rule of thumb the minimum spacing is three times the horizontal projection of the width of the pv panels. The latter relation is given by Equation 12 (Chakraborty et al., 2015).

$$d(m) = 3 * w * sin(\beta) \tag{12}$$

To calculate the total required area for the PV array, a module with the dimensions 1 by 2 [m] is assumed with a power output of 0.3 [kW] and hence an area of 2 [m^2] (the same rated power and dimensions as used in the biggest solar power plant, Pavagada) (Verdict Media, 2020). The parameters used are listed in Table 3. Per meter row 0.6 [kW] is assumed, two modules attached to each other. In turn, a power density per area could be calculated. For 100 [GW] an area of 1,133 [km^2] would be the minimum area required for a fixed tilt system. It should be mentioned that this does not yet include any area needed for power electronic support systems, nor for accessibility. The area depends mostly on the technology chosen (e.g. fixed tilt, single axis tracking, double axis tracking or opposite tilt orientation).

When comparing this area requirement to for instance the Abu Dhabi Noor Power Plant, the area requirement seems to be overestimated, since that power plant needs about 6.84 [km^2] per [GW]. As mentioned, this Noor Power Plant uses opposite tilt orientation and as a result requires less area for the same rated power. Nevertheless, an additional area of 6% is assumed after visual inspection of the Noor Power Plant orientation (Kennedy, 2019). This again translates into an area of 1,200 [km^2], hence about 24 by 50 [km]. The area that is needed for the subsequent stages in the supply chain that require a significant amount of land will be addressed in each specific cost model.

Initially Equation 14 will be used to calculate the intermediate $LCOE$. Of course it would make sense to use a more advanced LCOE model like the one proposed by Vartiainen et al. for instance (Vartiainen et al., 2019). The land lease costs are assumed to be 0.10 [$\$ \cdot m^{-2}$] (Costa, 2019). The total invested capital in the pv system is the sum of the capital expenditure for the modules and the balance of system costs, as indicated in Equation 13. The balance of system costs includes mounting, installation work, grid connection, cabling and other infrastructure elements. It does not include inverters, since these are not needed as the DC electricity could be directly fed to the electrolyzers with auxiliary power electronic equipment, which has not been fully included in the balance of system costs. Besides, the landlease costs are taken separately.

Table 3: PV array paramaters overview.

Width w	4 [m]
Angle β	25 [°]
Space between rows	5.1 [m]
Horizontal projection row	1.7 [m]
d	6.8 [m]
P_{module}	0.3 [kW]
Area module per meter row	4 $[\mathrm{m}^2 \cdot \mathrm{m}^{-1}]$
Power module per meter row	0.6 $[kW \cdot \mathrm{m}^{-1}]$
Power density per square meter	6.8/0.6*1.06 = 12 $[\mathrm{m}^2 \cdot \mathrm{kW}^{-1}]$

$$Invest_{pv}(\$/kWp) = Capex_{mod} + Capex_{bos} \tag{13}$$

$$LCOE(\$/kWh) = \frac{Invest_{total} * Annuity + Cost_{landlease} * \mathrm{Land}_{total} + Invest_{total} * OM}{ElectricityThroughput} \tag{14}$$

The yield of the system is estimated to be the capacity factor times the number of hours per year times the nominal power of the PV system (see Equation 15). However, since also the degradation of the modules should be considered, this is assumed to be included in the operation and maintenance costs.

$$Electricitythroughput(kWh) = capacityfactor * 8760 * P_{nominal} \tag{15}$$

Table 4: Solar pv parameters (Vartiainen et al., 2019; PVinsight, 2020; Verdict Media, 2020).

Efficiency	15.6 %
Depreciation period	25 [year]
OM	1% $[\mathrm{CAPEX}^{-1} \cdot \mathrm{year}^{-1}]$
$Capex_{bos}$	128 $[\$ \cdot \mathrm{kWp}^{-1}]$
$Capex_{mod}$	194 $[\$ \cdot \mathrm{kWp}^{-1}]$
$Invest_{base}$	321 $[\$ \cdot \mathrm{kWp}^{-1}]$
$Invest_{compare}$	1 [kWp]
$Invest_{scale}$	1
$Land_{base}$	12 $[m^2 \cdot \mathrm{kW}^{-1}]$

The costs that are assumed for the PV system are listed in Table 4. The $Invest_{\mathrm{base}}$ is composed of the capital expenditure for the modules as well as the balance of system. The operation and maintenance costs are assumed to be 1% $[\mathrm{CAPEX}^{-1} \cdot \mathrm{year}^{-1}]$ for 2019. The module $CAPEX$ is, just like the study of Vartiainen, based on the spot prices of pv modules. Vartiainen et al. assume the average spot price over the first half of 2019, which was 222 [$·kWp] (Vartiainen et al., 2019). The current weekly spot price is 188 [$·kWp] (PVinsight, 2020). An additional 5.5 $[\$ \cdot \mathrm{kWp}^{-1}]$ is added for freight and insurance of the modules, just like Variainen et al. assume. On the other hand, the balance of system costs are more difficult

to estimate. For this, the analysis conducted by Central Electricity Regulatory Commission of India (CERC) is taken, that show balance of system costs of 128 [$·kWp^{-1}], which is used for this analysis because India already has a very competitive market (Vartiainen et al., 2019).

3.4.4 Electrolyzer

This Section will describe what will be assumed for the electrolyzer echelon of the supply chain. The electroyzer capacity is scaled to meet the pv power output at all times and therefore has the rated power of the pv system minus the power output that is needed to cover the average electricity consumption by the compressor that is located on the Fahud Salt Basin. However, since the pv output power is not constant, this will affect the load factor of the electrolyzer, increasing its relative $CAPEX$ costs as well as the $varOPEX$ by being on and off all the time. On the other hand, the electrolyzer will operate most hours at partial load, therefore increasing its efficiency (Armijo & Philibert, 2020). Assumed is that the electrolyzer will perfectly follow the power output of the pv system, with no delay.

Due to the more widespread use of alkaline electrolyzers nowadays, as well as lower costs, it is this type of technology that is chosen for the analysis. The efficiency is assumed to be 83% for the HHV of hydrogen and the land requirements are 0.095 [$m^2 \cdot kWe^{-1}$] (IEA, 2019). The market for this type of electrolyzers is existent, however there is economies of scale to be achieved for installing a much larger system. Where the PV system and battery market has actually reached this [GW] scale, electrolyzers have not and therefore a lower cost factor is taken into account. A cost reduction potential is estimated to be below 400 [$\$ \cdot kWe^{-1}$] at [MW] scale. The [GW] scale is expected to lower costs even further to about 200 [$\$ \cdot kWe^{-1}$] (Graré, 2019). All the relevant electrolyzer parameters are listed in Table 5.

Table 5: Electrolyzer parameters (Graré, 2019; Engineeringtoolbox, 2019; Ali Keçebaş, 2019; Walker et al., 2018).

Efficiency (HHV)	83 %
Purity	99.95 %
$Pressure_{out}$	30 [bar]
Electricity	47.6 [$kWh \cdot kg_{H_2}^{-1}$]
Depreciation period	40 [year]
OM	0.7 % [$CAPEX^{-1} \cdot year^{-1}$]
$Invest_{base}$	200 [$·kW^{-1}]
$Invest_{compare}$	1 [kW]
$Invest_{scale}$	1
$Land_{base}$	0.095 [$m^2 \cdot kW^{-1}$]

3.4.5 Salt cavern storage

In order to ensure the availability of hydrogen feed for the liquefaction, as well as the shipping, two storage facilities are proposed. This improves the load factor of the liquefaction installation as well as ensuring a stable stream of liquid hydrogen at the sending terminal. Obviously, liquid hydrogen storage directly after the electrolyzer would be too costly since

the energy losses of liquefaction are high. Besides, gaseous tank storage is presumable too expensive as well in comparison to salt cavern storage (Stolzenburg & Mubbala, 2013).

Therefore, salt cavern storage costs would the preferred option when a system of 100 [GW] solar power is chosen. The costs amount 61.8 million Euro for 500,000 [m^3] of hydrogen at a pressure ranging between 100 and 200 [bar]. The lifetime is 30 years and the OM costs are 2 % (Wolf, 2015; Reuß, Grube, et al., 2019). This investment includes both the excavation work as well as the on site investment in infrastructure, compression et cetera.

The capacity of the salt cavern storage (before the liquefaction), is assumed to be scaled with the f_{prod}, because the pattern in hydrogen production follows the production of solar power (a capacity factor of 0.19). A multiple of two is used to overcome days of low production as well as variability in the solar power output. Besides it covers contingencies in the consecutive steps in the supply chain. Hence, a total of about 10 times the daily hydrogen production should be storable.

The temperature is assumed to be 293 [K], hence a total mass of storable hydrogen (making use of the ideal gas law) ranging between 3,899 [t] at 100 [bar] and 7,354 [t] at 200 [bar] is found (Wolf, 2015). Hence, it will be the difference between these two pressures that could be stored in the salt cavern that is 3,455 [t] per system. Subsequently, the scaling factor is assumed to be 0.28 due to the sharp reduction in specific costs when the system is scaled (Stolzenburg & Mubbala, 2013; Reuß et al., 2017). The 3,899 [t] hydrogen that always remains in the salt cavern at the lower limit, is called cushion gas, and is recovered at decommissioning.

Lastly, the area requirements are calculated by using a bird eye's view, a two-dimensional overlay of the salt cavern. As a result, with a typical diameter of 70 [m], a 3,848 [m^2] area is found per system (Wijk, 2019a). These two-dimensional overlays are usually constrained by the above ground situation (e.g. city, protected areas etc) (Caglayan et al., 2019). In Table 6, the parameters are summarized.

Table 6: Cavern storage parameters (Reuß et al., 2017; Reuß, Welder, et al., 2019).

Depreciation period	30 [year]
OM	2.0 % [$\text{CAPEX}^{-1} \cdot \text{year}^{-1}$]
$Invest_{base}$	68 E6 [$\cdot$system^{-1}]
$Invest_{compare}$	3.5 E6 [kg]
$Invest_{scale}$	0.28
$Land_{base}$	3.9 E3 [$m^2 \cdot \text{system}^{-1}$]

3.4.6 Compressor

This Section will describe what will be assumed for the compression echelon of the supply chain. Generally, the pressure level that is assumed after the electrolyzer is 30 [bar], whereas the pressure level before the pipeline is assumed to be 100 [bar]. Therefore, the pressure has to be increased. However, there are various ways in which a compression could take place and what energy it will require. Figure 27 indicates the energy that is required for an isothermal, adiabatic as well as a practical hydrogen compression. The practical hydrogen compression requires about the average of an isothermal and adiabatic compression.

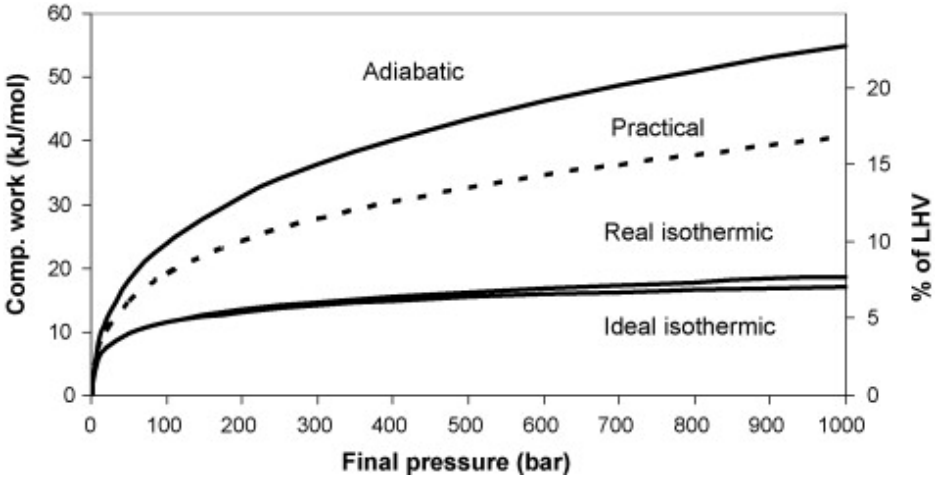

Figure 27: The energy that is needed for hydrogen compression at different required levels (Jensen et al., 2007).

All the hydrogen has to be compressed from 30 to 100 [bar] to feed it to the pipeline system. However, part of the hydrogen has to be compressed even further to 200 [bar] in order to inject it in the salt cavern. Since the capacity factor is 0.19 of the pv system, 19% of the hydrogen is directly fed to the pipeline system, and 81% of the hydrogen first goes through the salt cavern and hence has to be compressed to this increased pressure level of 200 [bar].

The work required to achieve an isothermic compression from 30 to 100 [bar] would be 0.39 $[kWh \cdot \mathrm{kg}^{-1}]$ hydrogen, at a temperature of 293.15 [K]. On the contrary, the work required to achieve this increase in pressure for an adiabatic compression would be 0.49 $[kWh \cdot \mathrm{kg}^{-1}]$ hydrogen, at a temperature of 293.15 [K]. According to Jensen et al. a practical compression would about the average of these two compressions (Jensen et al., 2007). Hence, it is assumed 0.44 $[kWh \cdot \mathrm{kg}^{-1}]$ is needed per [kg] of hydrogen. Taking into account the efficiency of 65%, this would translate into 0.68 $[kWh \cdot \mathrm{kg}^{-1}]$(Parks, 2014) which applies to every [kg] of hydrogen since everything has to be compressed too at least 100 [bar].

The 81% of the hydrogen that also goes through the salt cavern storage, has to be compressed further. The pressure level that is required depends on the actual pressure within the salt cavern. For simplicity, it is assumed that every [kg] of hydrogen that goes through the salt cavern has to be compressed to at least 200 [bar]. Hence, the pressure has to further increase from 100 to 200 [bar]. Following the same argumentation as in the previous paragraph and taking into account the same efficiency of 65%, this would translate into 0.37 $[kWh \cdot \mathrm{kg}^{-1}]$ for a practical compression.

The nominal capacity of the compressors is calculated in the following way. First the average is taken, so an average [kg] of hydrogen requires 0.98 $[kWh \cdot \text{kg}^{-1}]$ (0.67 plus the additional 0.37 for 81% of the hydrogen). Subsequently, the number of [kW] is determined by dividing the annual throughput of hydrogen by the number the number of [kg] hydrogen a one [kW] compressor could compress. Lastly, the nominal capacity is multiplied by a factor f_{prod} due to the irregular compression of hydrogen.

The $CAPEX$ assumed is found to be 4,290 $[\$ \cdot \text{kW}^{-1}]$, the lifetime is assumed to be 15 years, the scaling factor 0.8335 and finally the operation and maintenance costs are estimated to be 4% per annum of the total amount of capital invested (Heuser et al., 2019). An overview of the parameters is provided in Table 7.

Table 7: Compressor parameters (Reuß et al., 2017; Parks, 2014).

$Pressure_{in}$	30 [bar]
$Pressure_{out}$	100 [bar]
Efficiency	65 %
Depreciation period	15 [year]
OM	4 % $[\text{CAPEX}^{-1} \cdot \text{year}^{-1}]$
$Invest_{base}$	4,290 $[\$ \cdot \text{kW}^{-1}]$
$Invest_{compare}$	1 [kW]
$Invest_{scale}$	0.8335

3.4.7 Hydrogen pipeline infrastructure

In this Section the costs associated with the pipelines are considered. These costs depend mainly on the diameter of the pipeline. In turn, the diameter is dependent on the distance, demand (throughput) as well as the admissible pressure drop (Reuß et al., 2017).

The capacity that is needed from the pipeline is calculated making use of the throughput of hydrogen in the supply chain and the HHV of hydrogen. This translates into a power needed for the pipeline, which will determine the investment costs of the pipeline, since the flow of hydrogen will be stabilized by the salt cavern storage after the electrolyzer.

In Figure 28, the relation between the pipeline investment costs and the pipeline diameter is given as well as the relation with the hydrogen flow in [GW] of hydrogen. The investment costs of Mischner et al. is based on a discretization of the investment costs of natural gas pipelines with an additional 5% to compensate for an eventual increase in costs to transform these pipelines into hydrogen transporting pipelines (Mischner et al., 2015).

$$Invest(eur/m) = 1.05 * 278.24 * e^{D} \tag{16}$$

Subsequently, these costs are linearized by Welder et al. by fixing both the gas velocity to 10 [m/s] and the density to 5.7 $[\text{kg} \cdot \text{m}^{-3}]$ of hydrogen (Welder et al., 2019).

$$Invest(eur/m) = 0.180 * P + 408 \tag{17}$$

The linearization could be used as in Equation 17. In Equation 17 the capacity of the hydrogen pipeline is represented by P and has the unit [MW]. This leads to a slight overestimation at low pipeline capacities while introducing an underestimation at higher pipeline capacities in the order of 10 [GW] (Reuß, Welder, et al., 2019). The result of this linearization is given in Figure 28. One could notice this over- and underestimation in the right half of Figure 28.

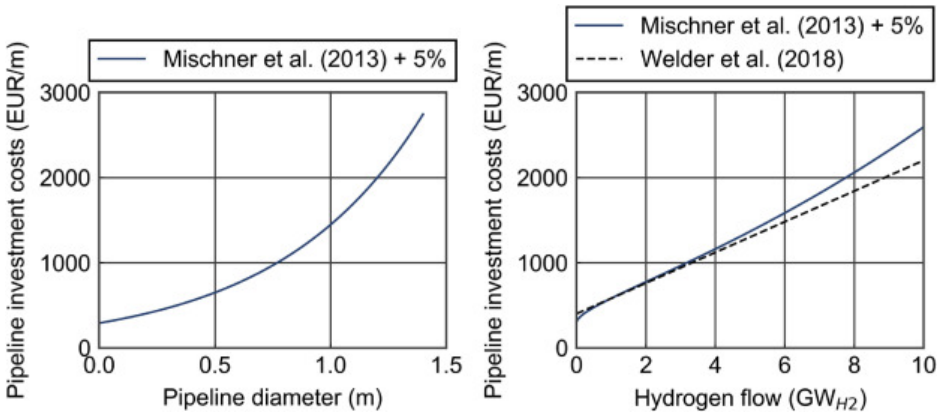

Figure 28: The pipeline diameter in relation to the pipeline investment costs and the relation between the pipeline capacity in [GW] versus the investment costs in [Eur/m] (Reuß, Welder, et al., 2019).

However, the velocity of hydrogen in natural gas pipelines could be higher than 10 [m/s], instead previous research shows that a velocity of 30 [$\mathrm{m} \cdot \mathrm{s}^{-1}$] is feasible, as it is currently in the United States (DNV GL, 2017). In addition, the 5% extra costs are presumably not needed since the pipelines are newly built (Wijk, 2019a). Therefore, Equation 16 is proposed without the 5% extra costs. In order to relate the investment costs and hence the diameter to the capacity of a pipeline, the relation in Equation 18 is used. The velocity v_{H2} is fixed to 25 [$\mathrm{m} \cdot \mathrm{s}^{-1}$], similar to previous research (Wijk, 2019a). The density ρ is 8 [$\mathrm{kg} \cdot \mathrm{m}^{-3}$] at 100 bar and 293.15 [K]. Finally, the E_{HHV} of 39.4 [$\mathrm{kWh} \cdot \mathrm{kg}^{-1}$] for hydrogen is used as well as the conversion from one [$\mathrm{kWh} \cdot \mathrm{kg}^{-1}$] to one [MJ], which is 3.6 [$\mathrm{MJ} \cdot \mathrm{kWh}^{-1}$].

$$D(m) = 2 * \sqrt{\frac{P_{MW}}{\pi * v_{H2} * \rho * E_{HHV} * 3.6}} \tag{18}$$

Subsequently, the required diameter from Equation 18 is plugged into Equation 16, without the 5% increase in costs but with conversion from USD to EUR.

Since the pv array is split into different blocks for accessability, where the 1 [GW] blocks are directly linked to the electrolyzers of the same capacity, pipelines are required from these blocks towards the salt cavern. About 2 [GW] of the pv system is needed for the the compressors to operate. Therefore, a total of 98 small pipelines is considered. The variability is not yet damped, therefore the combined capacity of these 98 pipelines is in total about 81 [GW].

As one could see in the Figure 17, Sohar is about 200 [km] from the closest salt basin, the Fahud Salt Basin. Therefore, a big pipeline over a distance of 200 [km] is needed to trans-

port the hydrogen from this salt cavern to the PoS. The cascading elements in the supply chain are assumed to operate at a 100% loadfactor. Besides, 5.5 [$\$\cdot m^{-1}$] for operation and maintenance costs would be considered and a depreciation period of 40 years (Reuß, Welder, et al., 2019). Finally, the remaining independent assumptions are given in Table 8.

Table 8: Pipeline parameters (Reuß, Welder, et al., 2019).

$Pressure_{in}$	100 [bar]
$Pressure_{out}$	80 [bar]
Depreciation period	40 [year]
OM	5.5 [$\$\cdot m^{-1}$]

3.4.8 Fuel cell

Since the hydrogen already is at base load at the receiving end of the pipeline, stationary PEM fuel cells are deployed to provide for stationary base load electricity to the liquefaction facility and the LH2 pump. The parameters used are listed in Table 9.

Table 9: Fuel cell parameters (Bruce et al., 2018; FCHEA, 2020).

Efficiency (HHV)	47 %
Depreciation period	20 [year]
OM	12.5 [$\$\cdot kWp^{-1} \cdot year^{-1}$]
$Invest_{base}$	568 [$\$\cdot kW^{-1}$]
$Invest_{compare}$	1 [kW]
$Invest_{scale}$	1
$Land_{base}$	0.40 [$m^2 \cdot kW^{-1}$]

3.4.9 Liquefaction

For the liquefaction installation, the following factors have been assumed and listed in Table 10 and Table 11. These parameters belong to the base case of a 50 [tpd] production facility. The actual feed pressure would be 80 [bar] at the receiving end after the pipeline, the $varOPEX$ of the liquefaction would be around 6 [$kWh \cdot kg^{-1}$] at 100% load conditions (Stolzenburg & Mubbala, 2013). Besides, the capital expenditure has a scaling factor of 0.66, based on Reuss et al. (Reuß et al., 2017). This means that only the $CAPEX$ is scaled and not the $varOPEX$, keeping the efficiency the same with rising output while reducing marginal capital costs.

With an assumed load factor of 100% and a feed pressure of 80 [bar], the electricity required for the feed compressor is no longer needed (0.74 [$kWh_{el} \cdot kg^{-1}$]), this would translate in a $varOPEX$ of 6.0 [$kWh_{el} \cdot kg^{-1}$]. In addition, the boil-off from Section 3.4.10 increases the capacity of the liquefaction, since also the storage boil-off needs be liquefied afterwards.

Table 10: Liquefaction parameters for a 50 tpd facility (Stolzenburg & Mubbala, 2013).

Operating load factor	Unit	100%	75%	50%	25%
Feed compressor	$[MWh_{el} \cdot \text{tLH2}^{-1}]$	0.74	0.76	0.77	0.81
Chiller	$[MWh_{el} \cdot \text{tLH2}^{-1}]$	0.11	0.11	0.11	0.11
Mixed refrigerant cycle	$[MWh_{el} \cdot \text{tLH2}^{-1}]$	0.66	0.66	0.66	0.66
Brayton cycles	$[MWh_{el} \cdot \text{tLH2}^{-1}]$	4.85	5.20	5.70	7.75
Flash gas cycle	$[MWh_{el} \cdot \text{tLH2}^{-1}]$	0.05	0.05	0.05	0.07
Total liquefaction process	$[MWh_{el} \cdot \text{tLH2}^{-1}]$	6.41	6.78	7.30	9.40
Auxiliaries	$[MWh_{el} \cdot \text{tLH2}^{-1}]$	0.35	0.40	0.49	0.79
Total liquefaction plant	$[MWh_{el} \cdot \text{tLH2}^{-1}]$	6.76	7.18	7.40	10.20

Table 11: Liquefaction parameters (U. Cardella et al., 2017).

Efficiency	42 %
Depreciation period	30 year
OM	3.0 % $[\text{CAPEX}^{-1} \cdot \text{year}^{-1}]$
$Invest_{base}$	1.155 E8 $[\$\cdot\text{system}^{-1}]$
$Invest_{compare}$	50 [tpd]
$Invest_{scale}$	0.66

3.4.10 Liquid storage

The second storage is located after the liquefaction plant. The output of the liquefaction plant is liquid hydrogen, therefore the second storage volume has to be in liquid form. This type of storage has been around for decades and is well developed. Since the temperature is close to 20 [K], it is very difficult to insulate the tank completely. Consequently, there will always be some boil-off gas, which rate is bigger at smaller volumes as the relative surface to volume ratio is bigger. However, at the size of that will be needed for this supply chain, the boil-off gas is about 0.003% per day (USdrive, 2017). The energy density of liquid hydrogen is about 71 $[\text{kg} \cdot \text{m}^{-3}]$ (Reuß et al., 2017).

Since the total mass of the assumed liquid hydrogen carrier is 11,360 [t], and the loading time is assumed to be 24 hours, the rate from the storage to the ship is about 473 $[t \cdot \text{hour}^{-1}]$. However, the amount of storage needed depends on the number of ships being used and the number of days the return trip from Sohar to Rotterdam takes plus the loading time. The number of ships depends again on the system size, since the size of the ship is fixed. At a system size of 100 [GW] solar, the production rate is 7,057 [tpd], which is still lower than the ship filling rate (which is 11,360 [tpd]). Besides, the number of ships is close to trip duration in days at a size of 100 [GW], which is beneficial as the liquid storage has to be overdimensioned too much otherwise.

Equation 19 is used to estimate the liquid storage size, with the number of buffer days set at two and the assumption that the tank could be filled at 100% capacity. The daily throughput is the daily hydrogen production. Finally, the area density of a sphere with a diameter of 45 [m] translates into an area density of 0.00072 $[\text{m}^2 \cdot \text{kg}^{-1}]$ (NCE, 2019). All parameter assumptions are listed in Table 12.

$$Capacity_{storage}(kg) = Capacity_{ship} + Buffer_{days} * throughput_{H2daily} \quad (19)$$

Table 12: Liquid storage parameters (Heuser et al., 2019; NCE, 2019).

Depreciation period	20 [year]
OM	2.0 % [CAPEX^{-1} · year^{-1}]
$Invest_{base}$	27.5 [\$·kg^{-1}]
$Invest_{compare}$	1 [kg]
$Invest_{scale}$	1
$Land_{base}$	0.00072 [$m^2 \cdot$ kg^{-1}]

To make up for contingencies, two buffer days are chosen initially, because it needs to have a capacity to overcome the time when there is no ship at the terminal. Since the loading time is assumed to be 24 [h], the time to store the daily production should be at least more than the trip time divided by the number of ships. As an example, when the trip time is 30 days, 15 ships are deployed and they sail exactly evenly on the route, there is 2 days between each ship on the route. With this one day loading time, there is no ship at the terminal for one day, therefore the liquid hydrogen has to store at least once the daily production without adjusting for contingencies.

The storage would cost 25 [€·kg^{-1}] hydrogen with OM costs of 2% of the $CAPEX$. Since perfect adiabatic conditions are impossible, a boil-off gas rate of 0.03% per day is assumed (Heuser et al., 2019). The boil-off gas is not lost, but instead fed back into the liquefaction plant, which hence requires a bigger liquefaction capacity. The amount of boil-off gas is determined by assuming the storage capacity is full all year long. The land base area density is based on the density of a sphere with a diameter of 45 [m], which translates into an area density of 0.00072 [m^2 · kg^{-1}] (NCE, 2019).

3.4.11 Liquid hydrogen pump

The pump that is needed to pump the hydrogen in the carrier has to be able to pump the hydrogen at a rate that fills the carrier in 24 [h], since that is the assumed loading time. Therefore, the pump needs a capacity that is able to pump all the hydrogen that has accumulated between ships arriving at the terminal in 24 [h]. This relation is given in Equation 20 where both the trip duration as well as the loading time are in hours. Furthermore, the cost factors assumed are provided in Table 13.

$$Capacity_{pump}(kg/day) = throughput_{H2daily} * \frac{tripduration + 2 * loadingtime}{24 * N_{ship}} \quad (20)$$

Table 13: Liquid hydrogen pump parameters (Reuß, Grube, et al., 2019).

Depreciation period	10 [year]
OM	3.0 % [$\text{CAPEX}^{-1} \cdot \text{year}^{-1}$]
Electricity demand	0.1 [$\text{kWh} \cdot \text{kg}^{-1}$]
$Invest_{base}$	33 [$\$\cdot\text{kg}^{-1}$]
$Invest_{compare}$	1 [$\text{kg} \cdot \text{day}^{-1}$]
$Invest_{scale}$	1
$Land_{base}$	0 [$m^2 \cdot \text{kg}^{-1}$]

3.4.12 Shipping

Equation 21 is proposed as the main formula used in order to calculate the number of ships (hence the costs of shipping). The number of ships N_{ship} is determined by the total hydrogen export, the capacity factor (to adjust for eventual variability of production with f_{cap}, which is set at 1.1), the duration of the trip (which is dependent on the speed and distance), the loading time as well as the capacity of the ship that is considered. Obviously, the number of ships is rounded upwards (Heuser et al., 2019).

$$N_{ship} = \frac{H2_{export} * f_{cap}}{capacity_{ship}} * \frac{tripduration + 2 * loadingtime}{8760} \tag{21}$$

Liquid hydrogen shipping The cost of shipping depends on the cost of the investment in a ship, the operational expenditure on the ship and the depreciation period. Liquid hydrogen shipping is chosen, as it offers flexibility for being used in different markets, while not requiring additional energy to be dehydrogenated as LOHCs do. According to Kamiya about 440 million USD would be reasonable per ship, carrying a capacity of 11,360 [t] of hydrogen and an operational expenditure of 2% (Kamiya et al., 2015).

Furthermore, the boil-off gas is assumed to be 0.2% and is fully deployed as the shipping fuel (Kamiya et al., 2015). Obviously, this boil-off gas will reduce the total amount of hydrogen received in Rotterdam, thereby increasing the levelized costs of hydrogen. On the other hand, it would diminish other propulsion fuel costs as these are no longer incurred. Hence, this is taken as a $varOPEX$ cost factor, with a theoretical cost of hydrogen of 2 [$\$\cdot\text{kg}^{-1}$].

The Kawasaki study assumes the amount of boil-off gas is enough to fuel the ship. In order to estimate whether the boil-off gas is sufficient to be used as the propulsion fuel, the following calculation is made. A large conventional LNG carrier of the type dual fuel diesel electric (DFDE) with a capacity of 160,000 [m^3], uses about 140 [t] of fuel per day (Ngai, 2018). The energy content of diesel is 12.22 [$kWh \cdot \text{kg}^{-1}$] (DNV GL, n.d.). Hence, 1,711 E3 [$kWh \cdot \text{day}^{-1}$] would be needed to power this LNG vessel. The efficiency is about 40 %, so only 684 E3 [$kWh \cdot \text{day}^{-1}$] is actually used to propel the ship (Tu, 2019).

A fuel cell efficiency of 47 % is assumed (HHV) (Bruce et al., 2018). This would translate into a hydrogen consumption of about 37 E3 [$\text{kg} \cdot \text{day}^{-1}$], considering the ship is empty on the return trip and therefore using less hydrogen, it is about the same as the on average 22.7 E3 [$\text{kg} \cdot \text{day}^{-1}$] that is due to boil-off hydrogen over the 14 days between the PoS and the

PoR for a single ship. Therefore, double the amount of boil-off is assumed to cover the fuel of the return trip as well.

Moreover, the loading time is assumed to be 24 hours at both the sending and receiving terminal. The trip duration is calculated from the distance between the PoR and PoS that is 11,218 [km] and divided by the assumed speed of 33 [km·h^{-1}] (Maritime Data Systems, 2019). This would translate into a duration of $\sim$ 30 days. Depending on the number of ships being used as well as the loading time, the number of terminals could be determined. When the number of ships exceeds the trip duration as well as the loading time, with a loading time of one day, an additional terminal would be needed.

3.4.13 Total cost of hydrogen

In this Section, the total costs of hydrogen will be described and decomposed into its constituents. The total costs could be calculated, and dividing them by the hydrogen throughput provides for a $LCOH$ by making use of Equation 22. The hydrogen throughput is adjusted for the hydrogen consumed at the stationary fuel cells as well as the hydrogen used during the shipping of the liquid hydrogen.

$$LCOH(\$/kg) = \frac{TOTEX_{system}}{Hydrogenthroughput} \tag{22}$$

4 Results

In this Chapter, the results will be covered. The price of hydrogen in [$\$ \cdot kg^{-1}$] has a sensitivity for each parameter used in the cost model introduced in Chapter 3. In Section 4.1, the energy balance is shown by means of a Sankey diagram. Furthermore, in Section 4.2 the size of each echelon in the supply chain is given. Moreover, in Section 4.3 the *LCOH* will be decomposed into its constituents. Thereafter, Section 4.4 provides for each relation between the hydrogen price and the price of one of the parameters.

4.1 Energy balance

In Figure 29, the energy balance is depicted for the HHV of one [kg] of hydrogen arriving in Rotterdam. It becomes clear that the overall efficiency of the supply chain is 58%. This number does not include the efficiency of the pv system itself, which was assumed to be 15.6% without further losses in the accompanying power electronic equipment. The biggest loss occurs at the hydrogen flow towards the fuel cell, since it has to provide the base load electricity to the liquefaction as well as the liquid hydrogen pump.

The fuel cell uses 13.8 [kWh] for every [kg] of hydrogen arriving in Rotterdam. This energy consumption is further split into the loss of energy due to the efficiency of the stationary fuel cell, which is assumed to be 47%, and the necessary energy to liquefy and pump hydrogen into to the carrier. Both liquefaction and the hydrogen pump require in this energy balance more energy in comparison to the base numbers assumed in Chapter 3, as the boil-off that is used as a shipping fuel has been liquefied as well and the balance is made for one kilogram to arrive.

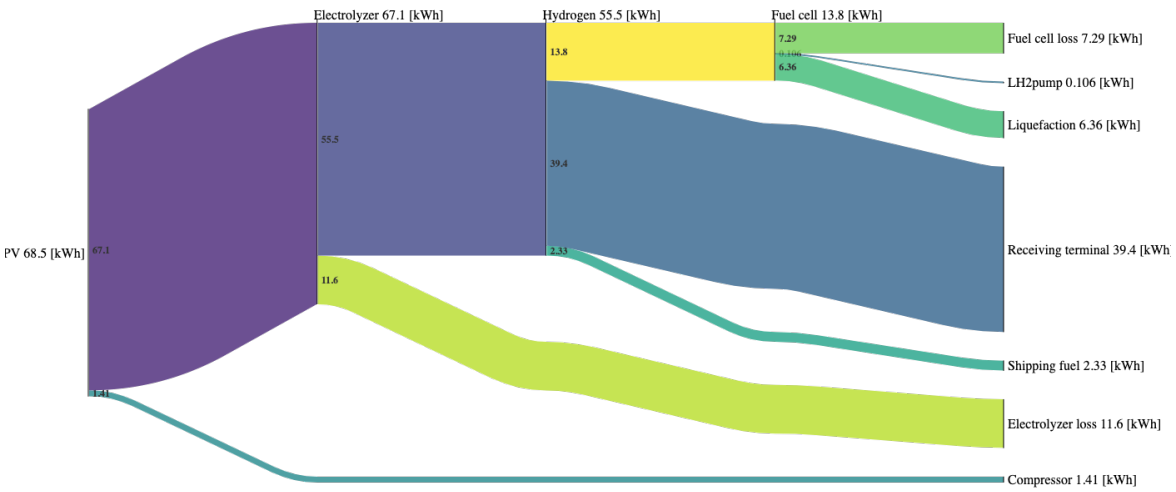

Figure 29: Sankey digagram showing the energy balance for one [kg] of green hydrogen received at the Port of Rotterdam.

The second biggest loss is due to the electrolyzer efficiency of 83% for the HHV of hydrogen. Hence, 11.6 [kWh] is lost. In addition, the boil-off gas during shipping further lowers the

efficiency of the supply chain, while also avoiding costs as no other shipping fuel is needed. Lastly, the compressor needs on average 0.98 [kWh] per [kg] of hydrogen. However, the mass of hydrogen that is used by the fuel cell as well as during the shipping has to be compressed as well. As a result, 1.41 [kWh] of energy is needed for compression of one [kg] of hydrogen to arrive in Rotterdam.

4.2 Sizing

In Table 14, the size of each system element is given. The units are provided as well. These sizes were used to scale the $CAPEX$, $fixOPEX$ and $varOPEX$ (for the $varOPEX$ the intermediate $LCOE$ was used or alternatively the $LCOH$ for shipping) . Besides, the total land requirements are calculated for the most land demanding stages in the supply chain, from its base land requirement. As assumed, the capacity of the electrolyzers is the capacity of the pv system minus the capacity of the pv system that is needed to power the compressors.

Table 14: Sizing and capacities of each stage.

Stage	$Capacity_{total}$	Daily volume (volume, mass or energy)	Volume type	$Land_{total}$ [ha]
Reverse osmosis	8.45e+04 $[m^3 \cdot day^{-1}]$	8.45e+04 $[m^3 \cdot day^{-1}]$	Production	35.3
Water pipeline	8.45e+04 $[m^3 \cdot day^{-1}]$	8.45e+04 $[m^3 \cdot day^{-1}]$	Average throughput	0
PV system	100 [GW]	456 $[GWh \cdot day^{-1}]$	Production	1.2e+05
Electrolyzer	97.9 [GW]	9.39 $[kt \cdot day^{-1}]$	Production	930
Pipeline small	80.8 [GW]	9.39 $[kt \cdot day^{-1}]$	Average throughput	0
Cavern storage	98.8 [kt]	9.39 $[kt \cdot day^{-1}]$	Average throughput	11
Compressor	2.02 [GW]	9.39 $[kt \cdot day^{-1}]$	Average throughput	0
Pipeline big	15.4 [GW]	9.39 $[kt \cdot day^{-1}]$	Average throughput	0
Fuel cell	1.8 [GW]	2.33 $[kt \cdot day^{-1}]$	Consumption	72.7
Liquefaction	7.07 $[kt \cdot day^{-1}]$	7.07 $[kt \cdot day^{-1}]$	Average throughput	0
Liquid storage	25.5 [kt]	7.06 $[kt \cdot day^{-1}]$	Average throughput	1.84
LH2pump	10.2 $[kt \cdot day^{-1}]$	7.06 $[kt \cdot day^{-1}]$	Average throughput	0
Shipping	21 [ships]	6.66 $[kt \cdot day^{-1}]$	Average throughput	0

To make it easier to interpret the numbers in Table 14, the following interpretations could be made. First of all, the reverse osmosis system system includes the CSP and the thermal energy storage. Furthermore, all the pipelines are considered to have a land base of zero as they need a much smaller area than for instance the pv system. The area needed for the electrolyzers within the pv system is about 0.8% of the land area.

The diameter of the small and big hydrogen pipelines is sized based on the hydrogen throughput. The diameter of the 98 small pipelines from the electrolyzer blocks towards the salt cavern is 0.19 [m]. On the other hand, the diameter of the big pipeline from the Fahud Salt Basin towards the PoS is 0.83 [m]. Both diameters are based on a pv system size of 100 [GW]. The liquefaction is sized about 141 times from the base 50 [tpd] system. The discrepancy between the total capacity of the liquefaction and the daily throughput after the liquefaction is due to the fact that the boil-off at the liquid storage is re-liquefied as well. The liquid storage could be interpreted as about 7 spheres of 3,500 [t] and a corresponding volume of 50 thousand [m^3] per sphere. Alternatively, it requires about 94 spheres of the size currently used by NASA. As a reference, Figure 23 could be perceived.

Another remarkable number is the capacity of the liquid hydrogen pump which is oversized compared to the average daily hydrogen throughput by about 44% due to the time in between loading time. In addition, the number of ships that is required to set up this supply chain is 20.7 and is rounded upwards to 21 ships in total.

Apart from the sensitivities of the price of hydrogen towards the costs incurred at each stage in the supply chain that are given in Section 4.4, all the base cost factors where used as they are introduced in Chapter 3. Consequently, the prices in Section 4.3 take into account these base cost factors. The total mass of hydrogen produced in the PoS is 2.58 [Mt] annually, which is about 7,058 [$t \cdot day^{-1}$]. In the PoR about 2.43 [Mt] would arrive annually, based on the 100 [GW] solar pv system. This translates into about 6,663 [$t \cdot day^{-1}$]. Hence, about 0.15 [Mt] of hydrogen is boil-off gas and used as a shipping fuel annually.

4.3 Decomposition price

The intermediate $LCOE$ is 0.013 [$\$ \cdot kWh^{-1}$] for the electricity coming from the pv system, taking into account the module costs, balance of system costs, OM and the land lease costs. The $varOPEX$ of subsequent stages that require electricity (e.g. liquefaction), is derived from this $LCOE$, but does not contribute to the $LCOH$ as the costs for the pv system are already covered in the $CAPEX$ and $OPEX$. The same is true for the $varOPEX$ incurred during shipping, as the boil-off is already deducted from the total throughput of hydrogen arriving in Rotterdam.

In Figure 30, the price built up is given by means of a waterfall chart. The absolute price is calculated and is found to be 2.17 [$\$ \cdot kg^{-1}$] of hydrogen arriving in the PoR. In order to get a better understanding of what the relative distributions are of the costs, these are provided as well. Four dominant cost factors are visible in decreasing order: pv system, electrolyzer, shipping and liquefaction. All the other cost factors are below 0.06 [$\$ \cdot kg^{-1}$].

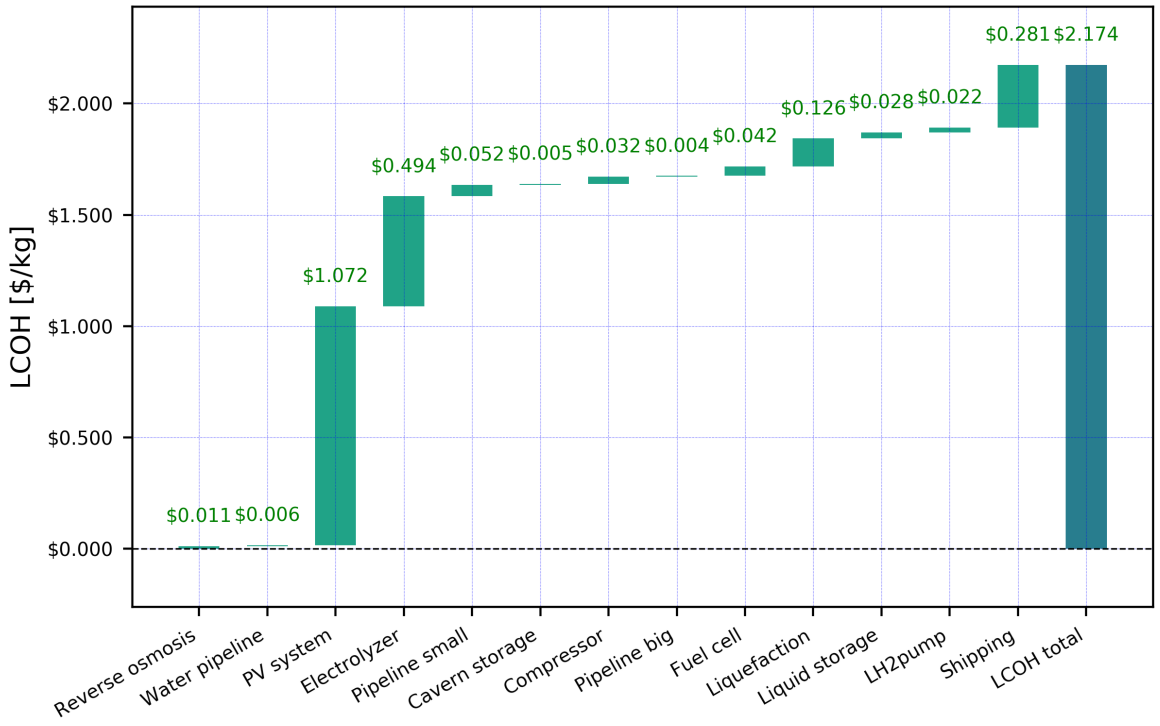

Figure 30: Decomposition of the LCOH into each stage in the supply chain in $[\$ \cdot \mathrm{kg}^{-1}]$.

In Figure 31, the price components are translated into the fraction that each stage adds to the $LCOH$. The biggest cost drivers become visible, which are in particular the pv system, the electrolyzer and the shipping. Nevertheless, the dominant factor is the pv system making up about 50% of the costs, which in turn is mostly $CAPEX$ dominated due to the module costs and balance of system. Put it differently, the four dominant cost factors pv system, electrolyzer, shipping and liquefaction make up about 91% of the total $LCOH$.

Finally, Table 16 shows the $Invest_{\text{total}}$, annuity, $CAPEX$, $fixOPEX$ and $varOPEX$. It could be found in Appendix B. These numbers correspond to the base situation: a pv system size of 100 [GW] and all the base prices also mentioned and described in Chapter 3.

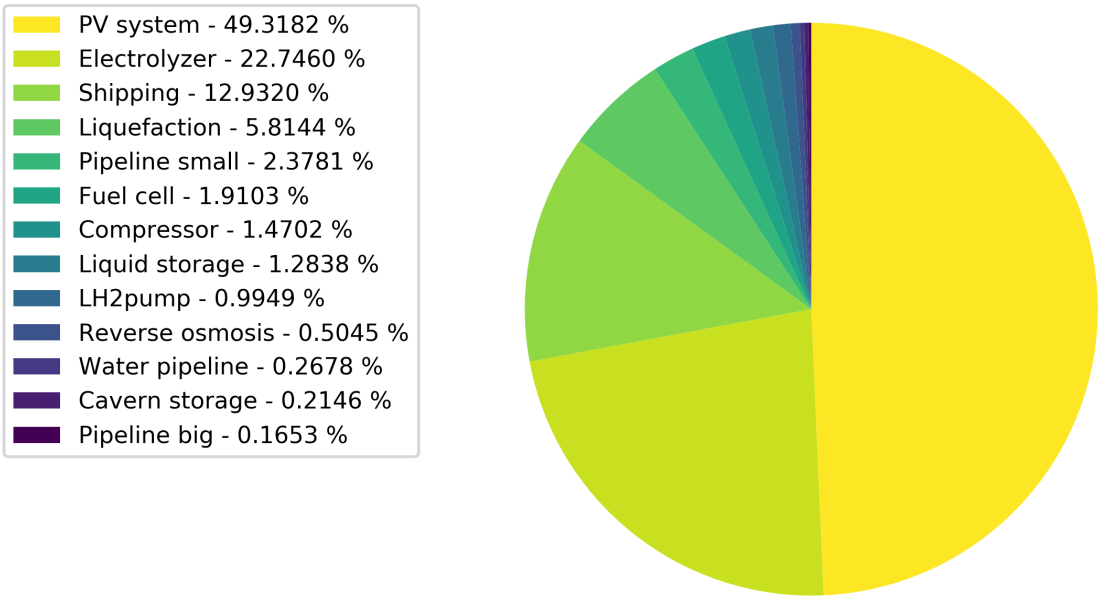

Figure 31: Contribution of constituents to the LCOH [%].

4.4 Sensitivity

In this Section the sensitivities will be analyzed. When altering the $CAPEX$ of the system on either the x or y axis, all the other supply chain cost factors are assumed to be the same. To put it differently, all the base cost factors from Chapter 3 are fixed. Obviously, the biggest reduction in $LCOH$ could be achieved when the the dominant cost factors become cheaper, either in the near future or when economies of scale are achieved within the very system itself when there would be a tender for instance. For that reason, the sensitivity of the $LCOH$ against the two most dominant cost factors is evaluated.

From Figure 30 it becomes clear that the pv system clearly is the biggest cost factor. The pv system costs are mostly determined by the $CAPEX$, which consist of both module and balance of system costs. Besides, the land lease costs and the OM are included in this price. The pv system also delivers power to the electrolyzers in order to produce hydrogen that is needed in the fuel cells. The power of the fuel cells is used in the liquefaction and the liquid hydrogen pump.

In Figure 32, the sensitivity of the price of the pv modules together with the system size and $LCOH$ is given, where a darker color represents a lower price. All the different supply chain elements are included in this price (e.g. shipping, liquefaction). The shipping is performed with liquefied hydrogen carriers. It does not include the costs of the receiving terminal. A 50% decrease in pv module costs is assumed as well as a system size ranging from 10% to 100% of the original 100 [GW] pv system. The scaling effects are effects are clearly visible. The lowest cost is achieved when the module price decreases by 50%, which causes the $LCOH$ to drop to about 1.8 $[\$ \cdot \mathrm{kg}^{-1}]$ when the 100 [GW] system is deployed.

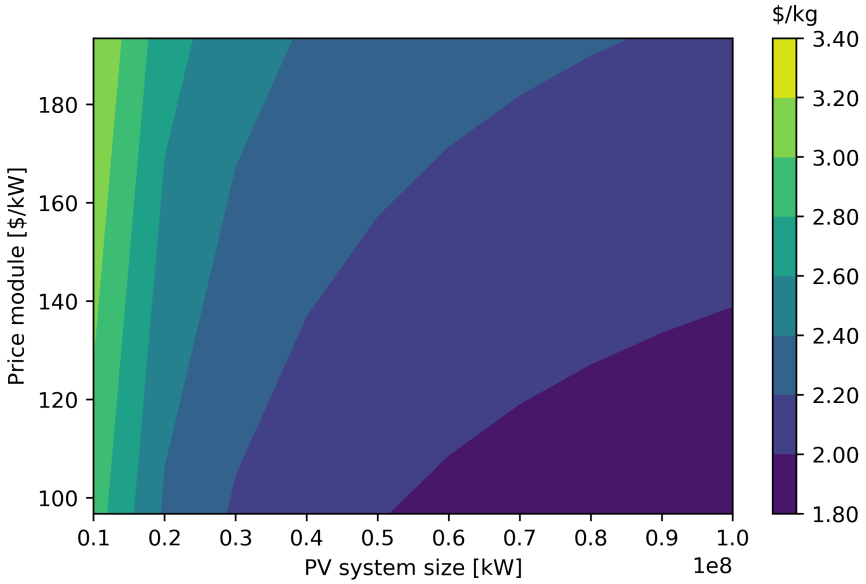

Figure 32: The relation between the size of the PV array in [kW], price of the pv module in $[\$ \cdot \mathrm{kW}^{-1}]$ and the price of green hydrogen in $[\$ \cdot \mathrm{kg}^{-1}]$.

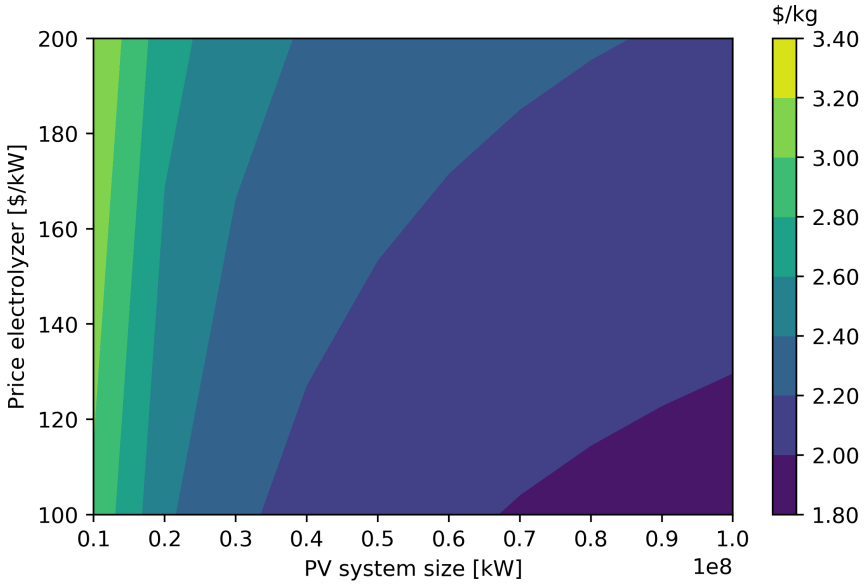

Figure 33: The relation between the size of the PV array in [kW], price of the electrolyzer stack in $[\$ \cdot \mathrm{kW}^{-1}]$ and the price of green hydrogen in $[\$ \cdot \mathrm{kg}^{-1}]$.

The sensitivity of the $LCOH$ to the price of an electrolyzer, the second biggest contributor to the $LCOH$, and the size of the system is the second relation plotted. Again, a 50% price decline is assumed and a system size ranging from 10 [GW] to 100 [GW]. In Figure 33, the sensitivity of the price of hydrogen is provided, where a darker color indicates again a lower price of hydrogen. It shows fairly similar behavior as the 50% cost reduction of the pv modules, however having a less pronounced effect. The cost reduction due to a 50%

decrease in module costs is more profound when comparing Figures 32 and 33, which is expected since it is a bigger cost contributing factor (even though here only a decrease in module costs is assumed and not in the other factors that contribute to the cost of solar pv such as land lease costs for instance). Again a $LCOH$ of about 1.8 [$\$ \cdot \mathrm{kg}^{-1}$] could be reached.

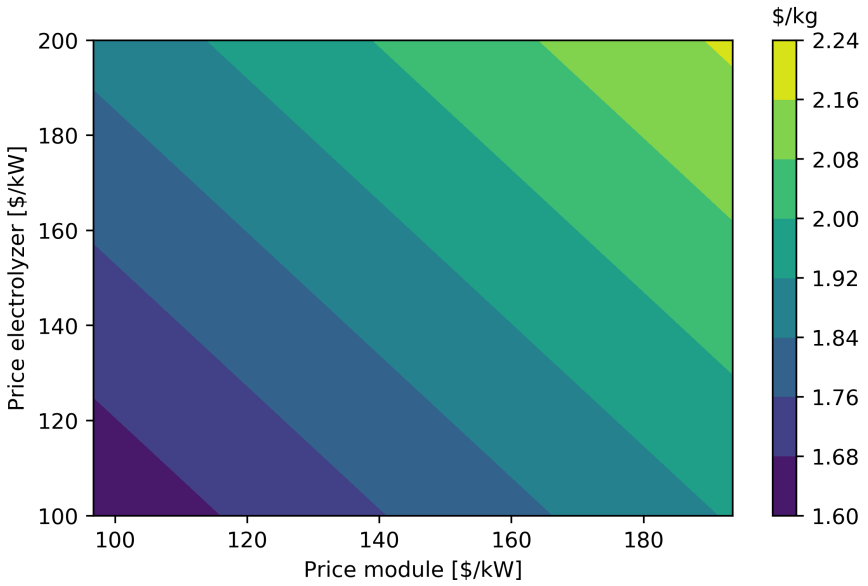

Figure 34: The relation between the price of the electrolyzer, pv module and the price of green hydrogen in [$\$ \cdot \mathrm{kg}^{-1}$].

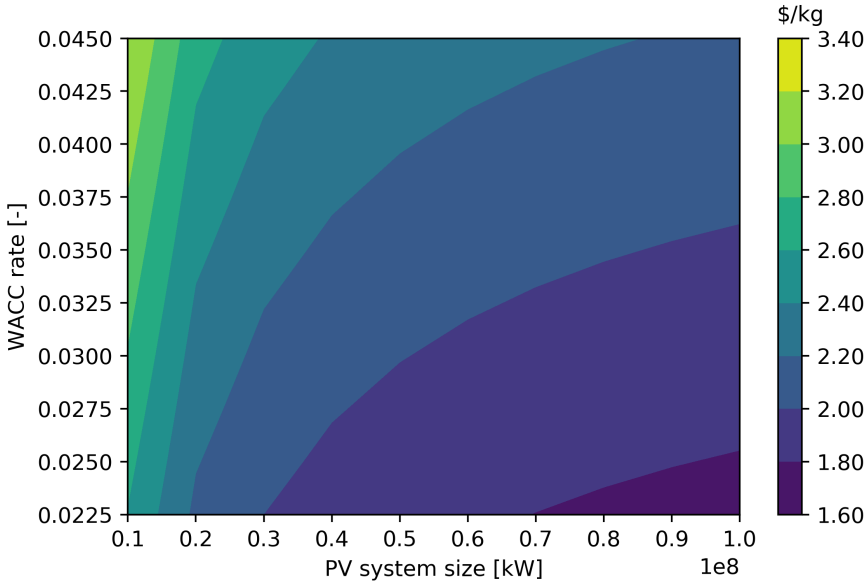

Figure 35: The relation between the nominal $WACC$, the pv system size and the price of green hydrogen in [$\$ \cdot \mathrm{kg}^{-1}$].

The third relation that is plotted is between the the main cost drivers: the pv module cost and the electrolyzer stack costs, while evaluating the $LCOH$ (see Figure 34). The same $CAPEX$ declines are assumed as in Figures 32 and 33. The scaling effects are no longer visible, since a fixed system size of 100 [GW] is taken. The lowest $LCOH$ is achieved when both the module and the electrolyzer costs decrease by 50%, and is found to be 1.62 [$\$ \cdot \mathrm{kg}^{-1}$].

The fourth and final relation is plotted in Figure 35. It depicts the sensitivity of the $LCOH$ to the $WACC$ and the pv system size. The $WACC$ is reduced by 50%. Keeping all the other factors constant, a 50% decrease in $WACC$ with a system size of 100 [GW] brings the $LCOH$ to again about 1.75 [$\$ \cdot \mathrm{kg}^{-1}$].

5 Discussion

In this Chapter, various relations, complexities, assumptions, limitations and other considerations will be addressed. First and foremost, the area around Fahud should be evaluated further in order to assess the site conditions that are needed for a pv system design. Similarly, a geologist should be involved in order to research the feasibility of hydrogen storage in salt caverns and the availability of land in Oman and the PoS needs to be verified. Accordingly, the influence of local policy schemes in Oman, such as the In Country Value (ICV) and the influence of export taxes, should be studied (Costa, 2019). Likewise, also an overhead factor should be considered. Albeit these considerations are straightforward, the next concerns should be carefully evaluated before drawing any conclusions.

Generally, it is hard to make a fair comparison for the price of green hydrogen produced in Sohar. In spite of deriving a price per kilogram of green hydrogen, it is rather complex where to put the point of comparison. Having the point of comparison in Sohar, it would make sense to make a comparison with grey hydrogen and a markup for a future emission penalty. The markup is easily found, since SMR plants typically emit 9.01 $[\mathrm{kg}_{CO2} \cdot \mathrm{kg}_{H2}^{-1}]$ (Collodi et al., 2017). With a price of 50 $[\$ \cdot \mathrm{t}_{CO2}^{-1}]$ it would be 0.45\$ for every [kg] of hydrogen. The point of comparison in Figure 30 is rather difficult, since putting this point after the big hydrogen pipeline (hence the green hydrogen would be at 80 [bar] in the PoS), is not simply possible. The pv system is partially covering also the energy requirement of the subsequent stages in the supply chain (e.g. fuel cell).

Having the point of comparison in Rotterdam, it would be argumentative to compare it to the price of hydrogen produced in the Netherlands. Even in this case, the comparison is hard to make since the hydrogen from Sohar is arriving in a liquid state (being potentially more valuable). After producing grey or blue hydrogen in the Netherlands, it should actually be liquefied for a fair comparison, depending however on the market application. Besides both grey and blue hydrogen are produced with a totally different technology, emitting CO_2 in either case as the capture rates for CO_2 are never 100% (Collodi et al., 2017). On the other hand, comparing it to electrolysis based on green electrolyzer seems to be fair, while the electrolyzers are likely having a higher capacity factor and therefore passing on the intermittancy problem of renewables to other parties active on the electricity grid.

Finally, also purity levels should be considered in the comparison. Electrolyzers produce hydrogen at a purity of about 99.95%, with oxygen polluting the hydrogen mostly. The oxygen is relatively easy to separate with a drier (Walker et al., 2018). On the contrary, SMR (the dominant production method for hydrogen) produces hydrogen at a purity of 95% for traditional installations, while newer designs have pressure swing adsorption that enable purity levels of 99% or higher (Jechura, 2015). It is illustrative for the considerations that should be made.

Nevertheless, the alkaline electrolyzers likely also require a high purity water supply. In this study, the water is supplied by a reverse osmosis plant where the output is drinking water quality. Therefore an additional demineralization step is needed that is not included in the current cost analysis. Also, a water buffer is likely needed between the reverse osmosis installation and the electrolyzers. It is however not expected that either factor would add substantial costs.

From a methodological perspective, it is important to note that the methodology by Heuser and Reuss is only partially adopted and where deemed necessary altered (Heuser et al., 2019; Reuß et al., 2017). This master thesis considered a stand-alone system. Consequently, the costs incurred at one stage (e.g. pv system), are covering the $varOPEX$ of another stage. In other words, the electricity that is needed for the compressors, liquefaction as well as the liquid hydrogen pumps is produced by the pv system. There might be synergies by connecting the proposed system to the national electricity grid in Oman, by providing stability to the grid at peak hours, or by using the electricity of the grid for the supply chain stages that need electricity to operate.

Ultimately, all the costs are attributed per [kg] of hydrogen by means of a $LCOH$. Land use has been added to the methodology for the most land demanding supply chain stages. The overcapacity factor f_{cap} was only used for calculating the required number of ships. Similar to Heuser et al., decommissioning costs have not been considered. Cushion gas, hydrogen that always remains in a storage unit, is assumed to be used at end-of-life (e.g. at the salt cavern, liquid storage and shipping storage tanks).

It is important to note that all the assumptions are based on present knowledge and hence present costs (inflation corrections were not applied). Cost factors, especially in renewable energy technologies, show very strong and unpredictable/volatile behavior. As a consequence, current cost estimates could soon be overhauled by rapid developments in pv technology, electrolyzer technology and other technologies assumed in this master thesis. Nevertheless, by taking present cost factors, the analysis is conducted as prudent as possible, while also showing sensitivities to the most contributing cost factors.

Besides, the sheer size of the system (100 [GW]) introduces further uncertainty, as the biggest pv power plant in the world is currently about 2 [GW], roughly 50 times smaller (Verdict Media, 2020). While for this master thesis a fixed tilt system is assumed, single axis tracking, double axis tracking as well as opposite tilt orientation based systems are developed as well. This has consequences for the capacity factor, but also for system costs. Again, to be prudent the most simple fixed tilt system is chosen.

Whereas global pv systems are in the order of gigawatts, present system sizes of electrolyzers are about a factor 1000 smaller in comparison to the system assumed for this research (FuelCellsWorks, 2019). Therefore, a lower cost estimate for electrolyzers is chosen of 200 $[\$ \cdot \text{kW}^{-1}]$ (Graré, 2019). Although it seems a fairly low $CAPEX$, technological progress is at a high pace as Chinese manufacturers indicate that they are able to reach this low $CAPEX$ already today (IRENA, 2019).

In addition, the OM rates are all percentages of the $CAPEX$. This is a fundamental assumption and not necessarily true when $CAPEX$ values change significantly. Hence, it might be better to assume certain absolute more specific values, similar to the pv system cost factor where also absolute OM values are assumed. Also, although OM is included in this analysis, the availability is assumed not to be affected and excluded from the analysis.

At the same time, even though partly represented in the scaling factors for compressors, cavern storage and liquefaction, economies of scale are not taken into account. For instance, even though wholesale pv module costs are considered, balance of system costs could poten-

tially show economies of scale as well. It should be noted that these balance of system costs are taken from one of the most competitive large scale pv system markets in the world, India.

Further power electronic equipment is included in this balance of system cost factor. On the other hand, power electronic equipment for the fuel cells as well as further auxiliary systems are not included in this analysis. In addition, Bruce et al. already indicate that for systems that are 100 [MW] or above (which is the case for this supply chain evaluation as well), either ammonia or hydrogen turbines are more likely to be deployed (Bruce et al., 2018). This market is not well developed and therefore fuel cells are the preferred option.

While pv system, pipelines, salt cavern storage and compressors are relatively well developed, liquefaction, liquid storage and liquid hydrogen carriers are less so at this system size. The liquefaction has to be about 141 times the daily mass throughput of a conceptual hydrogen liquefier proposed by IDEALHY (Stolzenburg & Mubbala, 2013). Liquid storage in this supply chain has about 94 times the capacity of the biggest liquid hydrogen storage in the world from NASA (NCE, 2019). Lastly, even though the liquid hydrogen carriers have been designed by Kawasaki (concepts) and the first liquid hydrogen carrier is launched, it takes time to develop these carriers from concepts to actually being operated. On the other hand, when these ships are developed and global trade in liquid hydrogen would develop accordingly, the green hydrogen supply chain could benefit from more frequent loading of ships that reduces the need for liquid hydrogen storage.

From Chapter 4, it becomes clear that the price of one [kg] of hydrogen sharply decreases with increasing system size. In other words, the scaling effects (see Equation 1) have a pronounced effect on the $LCOH$. These are partly due to the scaling factors assumed for the compressor, cavern storage and liquefaction. However, when only using scaling factors of 1 (hence zero induced scaling), the scaling still becomes apparent. A closer examination by plotting the waterfall chart for a 10 [GW] as well as a 100 [GW] system reveals that the scaling effects are only happening at the following supply chain elements: water pipeline, small and big hydrogen pipeline, liquefaction, liquid storage and finally the shipping.

All the other system elements do not have lower cost factors when the system is increased in size. In fact, these all stay exactly the same. The explanation for the scaling effects are different for the cost factors mentioned earlier. For the water pipeline, it is obvious that scaling effects are visible. It is the only supply chain element that is fixed, which means that the the size of the pipeline (hence the total invested capital) remains unaltered. When increasing the hydrogen throughput in the supply chain, these fixed costs are spread over more kilograms of hydrogen and as a result a lower $LCOH$ for the water pipeline is achieved.

It is less expected that the small and big hydrogen pipelines show scaling effects since the capacity of these pipelines grows with increasing throughput. A closer examination however reveals that relative costs per meter pipeline decrease when increasing its size, while also lowering the specific OM costs since a fixed cost factor per meter of pipeline is assumed.

The reason why the liquefaction shows scaling effects, might be unexpected. Nevertheless, it becomes clear when considering the following assumption in the cost model: the boil-off gas in the liquid hydrogen storage is fed back to the liquefaction. Since the liquid storage is partly determined by the ship size (which is fixed, see Equation 19), the boil-off per day is

relatively bigger for a smaller system size and therefore increasing the $LCOH$ contribution of the cost factor liquefaction. This also explains the bigger cost contribution of the liquid storage.

Lastly, the contribution to the $LCOH$ of shipping seems to be slightly bigger at a smaller system size. It is however due to the upward rounding of the number of ships when determining the number of ships needed to accomplish a dedicated supply chain. The same behavior is visible when decreasing the step size, showing an irregular pattern with increasing system size.

Yet there is ample opportunity for further cost reduction. The low capacity factor of the solar pv cascades through the supply chain. The electrolyzers, small pipelines, compressors and cavern storage all have to be overdimensioned due to this irregular load. The capacity factor of the power system could either be increased by using different technology (e.g. double axis tracking increases the capacity factor), or by introducing different resources to the system (e.g. wind power). Even though it might increase $CAPEX$, it might lower the $LCOH$ at the same time. Similarly, curtailment of the pv power might prove to be a solution to marginally increase pv power costs, but thereby increasing the capacity factors of cascading supply chain stages and thereby lowering both capital and operational costs. These trade-offs have to be analyzed further.

Another example of cost reduction would be increasing revenue from unused flows. With the production of every [kg] hydrogen, 8 [kg] of oxygen is produced. Even though oxygen is more readily available, as the concentration in air is relatively high, pure oxygen could eventually be sold to local industries. The revenue from oxygen sales could be up to 80 $[\$ \cdot \mathrm{t}^{-1}]$ (Breyer et al., 2015). However, the price is highly dependent on the value of oxygen to these local industries (Fasihi et al., 2016). Thereby oxygen sales could lower the $LCOH$ by up to 0.64 $[\$ \cdot \mathrm{kg}^{-1}]$ of hydrogen produced (Breyer et al., 2015). The costs of the pipeline as well as compression of oxygen are in this case neglected. Besides, the total amount of oxygen would be about 27.3 [Mt] for the 100 [GW] solar pv system. It would be unlikely that all this oxygen could be used in the PoS. Differently, in Chapter 2 an estimate of the current hydrogen demand is calculated to be be 1,163 $[\mathrm{t} \cdot \mathrm{day}^{-1}]$. This already is 16% of the hydrogen produced in the PoS before shipping. It would be desirable to fulfill this hydrogen demand first before shipping the hydrogen to Rotterdam.

Accordingly, the heat that is generated in the system could be harnessed. For instance the heat in the stationary fuel cells could be linked to local industries as low temperature heating in boilers (Bruce et al., 2018). Eventually, even the brine effluent could employed in the chlor-alkali industry (Reig et al., 2014).

From an operational perspective, it is yet unclear what operating regime would be favourable for the supply chain as a whole as well as specific supply chain elements. To illustrate this, the exact pressure at which to operate the salt cavern storage has to be simulated. Or it might be more advantageous for instance to have a several separate salt caverns at different pressures. More importantly, simulation of the supply chain and dynamic optimization could prove the feasibility of this conceptual supply chain and potentially lower costs. These simulations could also explore how resilient the supply chain is for seasonal variability. A further increase in hydrogen storage in salt caverns (it has a relatively low cost factor) could

for instance enable damping of seasonal solar influx variability, further stabilizing the supply chain. Therefore, future research could research this supply chain more extensively.

6 Conclusion and recommendations

The aim of this study was to evaluate the current techno-economic feasibility of a green hydrogen supply chain between the PoS and the PoR. This conceptual supply chain is based on solar pv as a resource solely, in combination with alkaline electrolyzers, hydrogen liquefaction plants and liquid hydrogen shipping. A literature analysis is conducted in order to evaluate the status quo regarding green hydrogen supply chains as well as technological- and cost developments in each technology that is needed to set up such a green hydrogen supply chain.

A cost model is proposed that included the $CAPEX$, $fixOPEX$ and $varOPEX$ of each supply chain stage. Furthermore, every technology has been sized to match the power output of the solar pv system. Hydrogen storage is included in order to lower the variability in the supply chain by means of salt cavern storage. Liquid hydrogen storage is included to buffer for contingencies as well as to overcome the time in between hydrogen carriers arriving in the PoS. The following conclusions could be drawn to address the main research question as well as the sub-questions.

First of all, from literature it becomes clear that there is no existent international green hydrogen supply chain, even though the costs have been evaluated for some theoretical supply chains. Concerning the main research question it seems technologically feasible to set up a green hydrogen supply chain between the PoS and the PoR. From an economic perspective, while addressing the fourth sub-question and assuming this 100 [GW] pv system and current costs, the $LCOH$ would be 2.17 [$\$ \cdot kg^{-1}$].

The $LCOH$ is lower in comparison to the cost estimate by the International Energy Agency (IEA) for imported hydrogen as well as domestic electrolysis green hydrogen production, which was found to be 3.1 [$\$ \cdot kg^{-1}$] for either case in Europe. Domestic production with renewables elecrolysis assumes $CAPEX$ of 450 [$\$ \cdot kW^{-1}$] for electrolyzers, 400 [$\$ \cdot kW^{-1}$] for solar pv and 900 [$\$ \cdot kW^{-1}$] for onshore wind (IEA, 2019). Comparing the $LCOH$ in this study to domestic grey hydrogen production, it would be proportionate to a domestic natural gas price of 5.6 [€$\cdot GJ^{-1}$] and a CO_2 price of about 75 [€$\cdot t^{-1}$] (Mulder et al., 2019).

Secondly, regarding the second and third sub-question, there is still a lot of uncertainty in order to asses the current techno-economic feasibility of a hydrogen supply chain between Sohar and Rotterdam. Both technological as well as economic assumptions have a profound impact on the price of green hydrogen arriving in Rotterdam. In order to reach a scale that is close to the envisioned demand of 2.4 [Mt] in Zuid Holland, at least 100 [GW] of solar pv needs to be deployed in Oman. In that case, 2.43 [Mt] of green hydrogen is received in Rotterdam annually. Transporting this amount requires 21 liquid hydrogen carriers of the bigger conceptual variant by Kawasaki to establish a dedicated green hydrogen trading link.

Thirdly, with respect to the fifth sub-question, the three cost factors that contribute the most to the price of green hydrogen sourced from Sohar are in descending order: pv system costs, electrolyzer costs and shipping costs. Therefore, future cost decline due to for instance economies of scale and learning curves likely has the biggest cost impact at respectively these three stages in the supply chain. Besides, from the sensitivity analysis could be concluded that reaching a 50% price decline in both electrolyzer and pv module $CAPEX$, a price of imported green hydrogen of 1.62 [$\$ \cdot kg^{-1}$] could be reached, which would be at par with the

price of grey hydrogen produced in the Netherlands following the assumptions by Mulder et al.. Furthermore, also the $WACC$ has a pronounced effect on the $LCOH$.

The following recommendations are proposed. Even though a green hydrogen supply chain using the configuration proposed in this master thesis results in a clear $LCOH$, there is ample opportunity for further cost reduction in this supply chain configuration. This research has been a first exploration. Therefore, future research could evaluate how this supply chain could further be optimized. In addition, the effects of economies of scale to the $LCOH$ should be evaluated. Besides, different green hydrogen routes should be studied using different hydrogen carriers.

References

Ahmed, M., Shayya, W. H., Hoey, D., & Al-Handaly, J. (2001). Brine disposal from reverse osmosis desalination plants in oman and the united arab emirates. *Desalination*, *133*(2), 135–147.

Albadi, M., Al-Badi, A., Al-Lawati, A., & Malik, A. (2011). Cost of pv electricity in oman. In *2011 ieee gcc conference and exhibition (gcc)* (pp. 373–376).

Ali Keçebaş, M. B., Muhammet Kayfeci. (2019). Retrieved from `https://www.sciencedirect.com/topics/engineering/alkaline-water-electrolysis`

Al-Kindi, M. H., & Richard, P. D. (2014). The main structural styles of the hydrocarbon reservoirs in oman. *Geological Society, London, Special Publications*, *392*(1), 409–445. Retrieved from `https://sp.lyellcollection.org/content/392/1/409/tab-figures-data` doi: 10.1144/sp392.20

Armijo, J., & Philibert, C. (2020, January). Flexible production of green hydrogen and ammonia from variable solar and wind energy: Case study of chile and argentina. *International Journal of Hydrogen Energy*, *45*(3), 1541–1558. Retrieved from `https://www.sciencedirect.com/science/article/abs/pii/S0360319919342089` doi: 10.1016/j.ijhydene.2019.11.028

Atlas, G. W. (2019). Retrieved from `https://globalwindatlas.info/area/Oman`

Ayodele, T., & Munda, J. (2019). Potential and economic viability of green hydrogen production by water electrolysis using wind energy resources in south africa. *International Journal of Hydrogen Energy*.

Bachner, G., Mayer, J., & Steininger, K. W. (2019). Costs or benefits? assessing the economy-wide effects of the electricity sector's low carbon transition–the role of capital costs, divergent risk perceptions and premiums. *Energy Strategy Reviews*, *26*, 100373.

Best, R. (2017). Switching towards coal or renewable energy? the effects of financial capital on energy transitions. *Energy Economics*, *63*, 75–83.

Breyer, C., Tsupari, E., Tikka, V., & Vainikka, P. (2015). Power-to-gas as an emerging profitable business through creating an integrated value chain. *Energy Procedia*, *73*, 182–189.

Bruce, S., Temminghoff, M., Hayward, J., Schmidt, E., Munnings, C., Palfreyman, D., & Hartley, P. (2018). National hydrogen roadmap. *Australia: CSIRO*.

Caglayan, D., Weber, N., Heinrichs, H. U., Linßen, J., Robinius, M., Kukla, P. A., & Stolten, D. (2019). *Technical potential of salt caverns for hydrogen storage in europe* (Tech. Rep.). Forschungszentrum Juelich GmbH, 52425 Juelich: Institute of Energy and Climate Research.

Cardella, U. (2019). *Large-scale liquid hydrogen production and supply advancing h mobility and clean energy.* Retrieved from `https://lngfutures.edu.au/wp-content/uploads/2019/10/Cardella-U.-Large-Scale-Liguid-H2-Production-and-Supply.pdf`

Cardella, U., Decker, L., & Klein, H. (2017). Economically viable large-scale hydrogen liquefaction. In *Iop conference series: materials science and engineering* (Vol. 171, p. 012013).

Cardella, U. F. (2018). *Large-scale hydrogen liquefaction under the aspect of economic viability* (Unpublished doctoral dissertation). Technische Universität München.

CBS. (2019, April). *Energieverbruik gedaald in 2018.* Centraal Bureau voor de Statistiek. Retrieved from `https://www.cbs.nl/nl-nl/nieuws/2019/16/energieverbruik-gedaald-in-2018`

Chakraborty, S., Sadhu, P. K., & Pal, N. (2015). Technical mapping of solar pv for ism-an approach toward green campus. *Energy Science & Engineering*, *3*(3), 196–206.

Cole, W. J., & Frazier, A. (2019). *Cost projections for utility-scale battery storage.*

Collodi, G., Azzaro, G., Ferrari, N., & Santos, S. (2017). Techno-economic evaluation of deploying ccs in smr based merchant h2 production with ng as feedstock and fuel. *Energy Procedia*, *114*, 2690–2712.

Costa, T. (2019, November). Personal communication.

Crotogino, F., Donadei, S., Bünger, U., & Landinger, H. (2010). Large-scale hydrogen underground storage for securing future energy supplies. In *18th world hydrogen energy conference* (Vol. 78, pp. 37–45).

Di Profio, P., Arca, S., Rossi, F., & Filipponi, M. (2009). Comparison of hydrogen hydrates with existing hydrogen storage technologies: Energetic and economic evaluations. *international journal of hydrogen energy*, *34*(22), 9173–9180.

DNV GL. (n.d.). *(future) fuels & fuel converters.* Retrieved from `https://www.ntnu.edu/documents/20587845/1266707380/01_Fuels.pdf/1073c862-2354-4ccf-9732-0906380f601e`

DNV GL. (2017). *Verkenning waterstofinfrastructuur.* Retrieved from `https://www.topsectorenergie.nl/sites/default/files/uploads/TKI%20Gas/publicaties/DNVGL%20rapport%20verkenning%20waterstofinfrastructuur_rev2.pdf`

Engineeringtoolbox. (2019). Retrieved from `https://www.engineeringtoolbox.com/fuels-higher-calorific-values-d_169.html`

Fasihi, M., Bogdanov, D., & Breyer, C. (2016). Techno-economic assessment of power-to-liquids (ptl) fuels production and global trading based on hybrid pv-wind power plants. *Energy Procedia*, *99*, 243–268.

FCHEA. (2020). *Fuel cell & hydrogen energy association.* Retrieved from `http://www.fchea.org/stationary`

Floodmap. (2019, January 9). Retrieved from `https://www.floodmap.net/Elevation/CountryElevationMap/?ct=OM`

Fraunhofer Institute. (2018). *Levelized cost of electricity renewable energy technologies.* Retrieved from `https://www.ise.fraunhofer.de/content/dam/ise/en/documents/publications/studies/EN2018_Fraunhofer-ISE_LCOE_Renewable_Energy_Technologies.pdf`

FuelCellsWorks. (2019, Sep). *Hamburg to build the world's largest hydrogen plant at its port - fuelcellsworks.* Retrieved from `https://fuelcellsworks.com/news/hamburg-to-build-the-worlds-largest-hydrogen-plant-in-its-port/`

Graré, L. (2019). *Hydrogen.*

Grigoriev, S., Porembsky, V., & Fateev, V. (2006). Pure hydrogen production by pem electrolysis for hydrogen energy. *International Journal of Hydrogen Energy*, *31*(2), 171–175.

Harding, R. (2019, December). *Japan launches first liquid hydrogen carrier ship.* Financial Times. Retrieved from `https://www.ft.com/content/8ae16d5e-1bd4-11ea-97df-cc63de1d73f4`

Heuser, P.-M., Ryberg, D. S., Grube, T., Robinius, M., & Stolten, D. (2019). Techno-economic analysis of a potential energy trading link between patagonia and japan based on co2 free hydrogen. *International Journal of Hydrogen Energy*, *44*(25), 12733–12747.

Huiting, H., & Vreeburg, J. (2020, January 6). Personal communication.

H-Vision. (2019, July). *Blue hydrogen as accelerator and pioneer for energy transition in the industry.*

IEA. (2015). *Technology roadmap hydrogen and fuel cells.* Retrieved from https://www.iea.org/publications/freepublications/publication/TechnologyRoadmapHydrogenandFuelCells.pdf

IEA. (2019). *The future of hydrogen.* Retrieved from https://www.g20karuizawa.go.jp/assets/pdf/The%20future%20of%20Hydrogen.pdf

IRENA. (2018). *Renewable power generation costs in 2018.* International Renewable Energy Agency, Abu Dhabi.

IRENA. (2019). *Hydrogen: A renewable energy perspective.* International Renewable Energy Agency, Abu Dhabi.

Jacobson, M. Z., & Jadhav, V. (2018, July). World estimates of pv optimal tilt angles and ratios of sunlight incident upon tilted and tracked pv panels relative to horizontal panels. *Solar Energy*, *169*, 55–66. doi: 10.1016/j.solener.2018.04.030

Jechura, J. (2015). *Hydrogen from natural gas via steam methane reforming (smr).* Retrieved from https://inside.mines.edu/~jjechura/EnergyTech/07_Hydrogen_from_SMR.pdf

Jensen, J. O., Vestbø, A. P., Li, Q., & Bjerrum, N. (2007). The energy efficiency of onboard hydrogen storage. *Journal of Alloys and Compounds*, *446*, 723–728.

Kamiya, S., Nishimura, M., & Harada, E. (2015). Study on introduction of co2 free energy to japan with liquid hydrogen. *Physics Procedia*, *67*, 11–19.

Kawasaki. (2019, September 27). *Kawasaki hydrogen road.* Presentation.

Kazem, H. A., Al-Waeli, A. H. A., Al-Kabi, A. H. K., & Al-Mamari, A. (2015). Technoeconomical assessment of optimum design for photovoltaic water pumping system for rural area in oman. *International Journal of Photoenergy*, *2015*, 1–8. Retrieved from https://www.hindawi.com/journals/ijp/2015/514624/ doi: 10.1155/2015/514624

Kennedy, M. (2019, Jul). *Abu dhabi throws the switch on world's largest single-site solar project.* Retrieved from https://newatlas.com/abu-dhabi-worlds-largest-single-site-solar-project/60463/

Laissaoui, M., Palenzuela, P., Eldean, M. A. S., Nehari, D., & Alarcón-Padilla, D.-C. (2018). Techno-economic analysis of a stand-alone solar desalination plant at variable load conditions. *Applied Thermal Engineering*, *133*, 659–670.

Lauer, M. (2008). *Methodology guideline on techno economic assessment (tea) generated in the framework of thermalnet wp3b economics.* Retrieved from https://ec.europa.eu/energy/intelligent/projects/sites/iee-projects/files/projects/documents/thermalnet_methodology_guideline_on_techno_economic_assessment.pdf

Macrotrends. (2019). Retrieved from https://www.macrotrends.net/2515/1-year-libor-rate-historical-chart

Maritime Data Systems. (2019). *Searoutes.* Retrieved from https://www.searoutes.com/routing?speed=13&panama=true&suez=true&kiel=true&rivers=block&roads=block

Melieste, R. (2017, November). *Deep decarbonization in the port of rotterdam.* Retrieved from https://www.voltachem.com/images/uploads/FINAL_VoltaChem_event_-_Presentatie_Port-of-Rotterdam.pdf ((Accessed on 06/10/2019))

Melieste, R. (2019, December). *Energiebalansen 2018.* ((Accessed on 27/12/2019))

Michalski, J., Bünger, U., Crotogino, F., Donadei, S., Schneider, G.-S., Pregger, T., ... Heide, D. (2017). Hydrogen generation by electrolysis and storage in salt caverns: potentials, economics and systems aspects with regard to the german energy transition.

International Journal of Hydrogen Energy, *42*(19), 13427–13443.

Mischner, J., Fasold, H.-G., & Heymer, J. (2015). *Gas2energy. net: Systemplanerische grundlagen der gasversorgung inkl. ebook*. Deutscher Industrieverlag.

Mohan, S. V., Sravan, J. S., Butti, S. K., Krishna, K. V., Modestra, J. A., Velvizhi, G., ... Pandey, A. (2019). Microbial electrochemical technology: emerging and sustainable platform. In *Microbial electrochemical technology* (pp. 3–18). Elsevier.

Mulder, M., Perey, P., & Moraga, J. L. (2019). *Outlook for a dutch hydrogen market: economic conditions and scenarois*. Centre for Energy Economics Research, University of Groningen.

NCE. (2019). *Norwegian future value chains for liquid hydrogen.* Retrieved from `https://maritimecleantech.no/wp-content/uploads/2016/11/Report-liquid-hydrogen.pdf`

Ngai, S. (2018). *Fuel efficiency demands shorten lng vessels.* Retrieved from `https://safetyatsea.net/news/2018/fuel-efficiency-demands-shorten-lng-vessels-lifespan/`

Niermann, M., Drünert, S., Kaltschmitt, M., & Bonhoff, K. (2019). Liquid organic hydrogen carriers (lohcs)–techno-economic analysis of lohcs in a defined process chain. *Energy & Environmental Science*, *12*(1), 290–307.

Papadopoulos, V., Desmet, J., Knockaert, J., & Develder, C. (2018). Improving the utilization factor of a pem electrolyzer powered by a 15 mw pv park by combining wind power and battery storage–feasibility study. *International Journal of Hydrogen Energy*, *43*(34), 16468–16478.

Parks, G. (2014). *Hydrogen station compression, storage, and dispensing technical status and costs*. National Renewable Energy Laboratory.

Pollastro, R. M. (1999). *Ghaba salt basin province and fahud salt basin province, oman: Geological overview and total petroleum systems*. US Department of the Interior, US Geological Survey.

Port of Rotterdam. (2017). *Zero-emission port by 2050 — port of rotterdam.* Retrieved from `https://www.portofrotterdam.com/en/news-and-press-releases/zero-emission-port-by-2050` ((Accessed on 06/17/2019))

PVinsight. (2020). Retrieved from `http://pvinsights.com/`

Reig, M., Casas, S., Aladjem, C., Valderrama, C., Gibert, O., Valero, F., ... Cortina, J. L. (2014). Concentration of nacl from seawater reverse osmosis brines for the chlor-alkali industry by electrodialysis. *Desalination*, *342*, 107–117.

Reuß, M., Grube, T., Robinius, M., Preuster, P., Wasserscheid, P., & Stolten, D. (2017). Seasonal storage and alternative carriers: A flexible hydrogen supply chain model. *Applied energy*, *200*, 290–302.

Reuß, M., Grube, T., Robinius, M., & Stolten, D. (2019). A hydrogen supply chain with spatial resolution: Comparative analysis of infrastructure technologies in germany. *Applied Energy*, *247*, 438–453.

Reuß, M., Welder, L., Thürauf, J., Linßen, J., Grube, T., Schewe, L., ... Robinius, M. (2019). Modeling hydrogen networks for future energy systems: A comparison of linear and nonlinear approaches. *International Journal of Hydrogen Energy*, *44*(60), 32136–32150.

Reuters Editorial. (2019, December). *Offshore wind developer orsted secures money for renewable hydrogen project.* Reuters. Retrieved from `https://www.reuters.com/article/us-orsted-renewables-hydrogen/offshore-wind-developer-orsted-secures-money-for-renewable-hydrogen-project-idUSKBN1YO0WC`

Rhino Energy. (2016). *Impact of shading.* Retrieved from http://www.greenrhinoenergy.com/solar/performance/shading.php

Samadi, S., Lechtenböhmer, S., Schneider, C., Arnold, K., Fischedick, M., Schüwer, D., & Pastowski, A. (2017a). *Decarbonization pathways for the industrial cluster of the port of rotterdam.*

Samadi, S., Lechtenböhmer, S., Schneider, C., Arnold, K., Fischedick, M., Schüwer, D., & Pastowski, A. (2017b). *Decarbonization pathways for the industrial cluster of the port of rotterdam.*

Satyapal, S. (2017). Hydrogen and fuel cells overview. In *Dla worldwide energy conference, national harbor, md.*

Schmidt, O., Gambhir, A., Staffell, I., Hawkes, A., Nelson, J., & Few, S. (2017). Future cost and performance of water electrolysis: An expert elicitation study. *International journal of hydrogen energy*, *42*(52), 30470–30492.

Shedid, M. H., & Elshokary, S. (2015). Hydrogen production from an alkali electrolyzer operating with egypt natural resources. *Smart Grid and Renewable Energy*, *6*(01), 14.

Steffen, B. (2019). *Estimating the cost of capital for renewable energy projects* (Tech. Rep.). Haldeneggsteig 4, 8092 Zurich, Switzerland: ETH Zürich.

Stolzenburg, ., & Mubbala, R. (2013). *Integrated design for demonstration of efficient liquefaction of hydrogen (idealhy) fuel cells and hydrogen joint undertaking (fch ju) grant agreement number 278177 title: Hydrogen liquefaction report.* Retrieved from https://www.idealhy.eu/uploads/documents/IDEALHY_D3-16_Liquefaction_Report_web.pdf

Syed, M., Sherif, S., Veziroglu, T., & Sheffield, J. W. (1998). An economic analysis of three hydrogen liquefaction systems. *International Journal of Hydrogen Energy*, *23*(7), 565–576.

Tarkowski, R. (2019). Underground hydrogen storage: Characteristics and prospects. *Renewable and Sustainable Energy Reviews*, *105*, 86–94.

Tesla. (2019, July). Retrieved from https://www.tesla.com/nl_NL/blog/introducing-megapack-utility-scale-energy-storage?redirect=no

Touili, S., Merrouni, A. A., Azouzoute, A., El Hassouani, Y., & Amrani, A.-i. (2018). A technical and economical assessment of hydrogen production potential from solar energy in morocco. *International Journal of Hydrogen Energy*, *43*(51), 22777–22796.

Tu, H. (2019). Options and evaluations on propulsion systems of lng carriers. In *Propulsion systems.* IntechOpen.

USdrive. (2017). *Hydrogen delivery technical team roadmap.* Retrieved from https://www.energy.gov/sites/prod/files/2017/08/f36/hdtt_roadmap_July2017.pdf

Van Den Bosch, F. A., Hollen, R., Volberda, H. W., & Baaij, M. G. (2011). The strategic value of the port of rotterdam for the international competitiveness of the netherlands: A first exploration. *Erasmus University Rotterdam, Rotterdam School of Management (RSM). Rotterdam: Port of Rotterdam*.

Vartiainen, E., Masson, G., Breyer, C., Moser, D., & Román Medina, E. (2019). Impact of weighted average cost of capital, capital expenditure, and other parameters on future utility-scale pv levelised cost of electricity. *Progress in Photovoltaics: Research and Applications*.

Verdict Media. (2020). *Pavagada solar park, tumkur district, karnataka, india.* Retrieved from https://www.power-technology.com/projects/pavagada-solar-park-karnataka/

Vreuls. (2004). *The netherlands list of fuels and standard co2 emission factors.* Retrieved from https://www.rvo.nl/sites/default/files/2013/10/Vreuls%202005%20NL%20Energiedragerlijst%20-%20Update.pdf

Walker, I., Madden, B., & Tahir, F. (2018). *Hydrogen supply chain evidence base.* Element Energy Ltd. Retrieved from https://assets.publishing.service.gov.uk/government/uploads/system/uploads/attachment_data/file/760479/H2_supply_chain_evidence_-_publication_version.pdf

Welder, L., Stenzel, P., Ebersbach, N., Markewitz, P., Robinius, M., Emonts, B., & Stolten, D. (2019). Design and evaluation of hydrogen electricity reconversion pathways in national energy systems using spatially and temporally resolved energy system optimization. *International Journal of Hydrogen Energy*, *44*(19), 9594–9607.

Weterings, R. (2019, October 11). *Terugkoppeling waterstofmissie japan.* Presentation.

Wijk, A. v. (2019a, September). *Hydrogen, the bridge between africa and europe.*

Wijk, A. v. (2019b, February). *Naar een groene waterstofeconomie in zuid-holland.*

Wolf, E. (2015). Large-scale hydrogen energy storage. In *Electrochemical energy storage for renewable sources and grid balancing* (pp. 129–142). Elsevier.

Worldbank. (2019). Retrieved from https://data.worldbank.org/indicator/AG.LND.PRCP.MM

Yasui, M. (2018, September). *Large-scale hydrogen storage and transportation system.* Retrieved from http://4echile.cl/4echile/wp-content/uploads/2018/09/OK_P21_Block-5_Makoto-Yasui_Chiyoda.pdf

Appendices

A Overview assumptions

Table 15: Overview of the assumptions for each supply chain stage.

	Reverse osmosis	Water pipeline	PV system	Electrolyzer	Pipeline small	Cavern storage	Compressor
State_in	Sea water	Permeate water	Irradiance	e- DC	30 [bar]	100-200 bar	30 [bar]
State_out	Permeate water	Permeate water	e- DC	30 [bar]	30 [bar]	100-200 bar	100 [bar] / 200 [bar]
Invest_base	11076361	1100000	321	200	371	67980000	4290
Invest_compare	35000	1	1	1	1	3455000	1
Invest_scale	1	1	1	1	1	0.28	0.834
Depreciation_period	1.05	40	25	40	40	30	15
OM	0	0.01	0.01	0.007	0.0148	0.02	0.04
Cost_demand	0	0	0	0	0	0	0.98
Land_base	146313	0	12	0.095	0	3.85e+03	0

	Pipeline big	Fuel cell	Liquefaction	Liquid storage	LH2pump	Shipping	
State_in	100 [bar]	30 [bar]	80 [bar]	2 [bar] LH2	2 [bar] LH2	2 [bar] LH2	
State_out	100 [bar]	e- DC	2 [bar] LH2	2 [bar] LH2	2 [bar] LH2	2 [bar] LH2	
Invest_base	703	568	1.16e+08	27.5	33	40000000	
Invest_compare	1	1	50	1	1	11360	
Invest_scale	1	1	0.66	1	1	1	
Depreciation_period	40	20	30	20	10	30	
OM	0.00782	0.022	0.04	0.02	0.03	0.02	
Cost_demand	0	0	6.01	0	0.1	0	
Land_base	0	0.405	0	0.000723	0	0	

B Overview cost factors

Table 16: Overview of the different cost factors.

Stage	Invest_total	Annuity	Capex	FixOPEX	VarOPEX	TOTEX	Fraction
Reverse osmosis	2.67e+07	0.996	0.011	1.45e-05	0	0.011	0.00505
Water pipeline	220000000	0.0543	0.00492	0.000905	0	0.00582	0.00268
PV system	3.21e+10	0.0674	0.891	0.181	0	1.07	0.493
Electrolyzer	1.96e+10	0.0543	0.438	0.0568	0	0.494	0.227
Pipeline small	1.82e+09	0.0543	0.0406	0.0111	0	0.0517	0.0238
Cavern storage	1.74e+08	0.0614	0.00439	0.000276	0	0.00466	0.00215
Compressor	7.72e+08	0.0931	0.0295	0.00241	0.0127	0.032	0.0147
Pipeline big	1.41e+08	0.0543	0.00314	0.000452	0	0.00359	0.00165
Fuel cell	1.02e+09	0.0769	0.0323	0.00926	0	0.0415	0.0191
Liquefaction	3.03e+09	0.0614	0.0765	0.0499	0.0782	0.126	0.0581
Liquid storage	7.01e+08	0.0769	0.0221	0.00576	0.00229	0.0279	0.0128
LH2pump	3.36e+08	0.126	0.0175	0.00415	0.0013	0.0216	0.00995
Shipping	8.4e+09	0.0614	0.212	0.0691	0.118	0.281	0.129
Total	NaN	NaN	NaN	NaN	NaN	2.17	1